

AperTO - Archivio Istituzionale Open Access dell'Università di Torino

Targeting Myeloid Differentiation Using Potent 2-Hydroxypyrazolo[1,5- a]pyridine Scaffold-Based Human Dihydroorotate Dehydrogenase Inhibitors

This is a pre print version of the following article:

Original Citation:

Availability:

This version is available <http://hdl.handle.net/2318/1686360> since 2019-01-10T01:05:46Z

Published version:

DOI:10.1021/acs.jmedchem.8b00373

Terms of use:

Open Access

Anyone can freely access the full text of works made available as "Open Access". Works made available under a Creative Commons license can be used according to the terms and conditions of said license. Use of all other works requires consent of the right holder (author or publisher) if not exempted from copyright protection by the applicable law.

(Article begins on next page)



UNIVERSITÀ DEGLI STUDI DI TORINO

This is an author version of the contribution published on:

Questa è la versione dell'autore dell'opera: Sainas, Stefano; Pippione, Agnese C; Lupino, Elisa; Giorgis, Marta; Circosta, Paola; Gaidano, Valentina; Goyal, Parveen; Bonanni, Davide; Rolando, Barbara; Cignetti, Alessandro; Ducime, Alex; Andersson, Mikael; Järvå, Michael; Friemann, Rosmarie; Piccinini, Marco; Ramondetti, Cristina; Buccinnà, Barbara; Al-Karadaghi, Salam; Boschi, Donatella; Saglio, Giuseppe; Lolli, Marco L.
Targeting Myeloid Differentiation Using Potent
2-Hydroxypyrazolo[1,5-a]pyridine Scaffold-Based Human Dihydroorotate
Dehydrogenase (hDHODH) Inhibitors
Journal of Medicinal Chemistry **2018**, 61 (14), 6034-6055.

The definitive version is available at:

La versione definitiva è disponibile alla URL:

<http://dx.doi.org/10.1021/acs.jmedchem.8b00373>

Targeting Myeloid Differentiation Using Potent 2-Hydroxypyrazolo[1,5-a]pyridine Scaffold-Based *Human* Dihydroorotate Dehydrogenase (hDHODH) Inhibitors

*Stefano Sainas,^a Agnese C. Pippione,^a Elisa Lupino,^b Marta Giorgis,^a Paola Circosta,^{c,d} Valentina Gaidano,^{e,f} Parveen Goyal,^g Davide Bonanni,^a Barbara Rolando,^a Alessandro Cignetti,^{e,f} Alex Ducime,^a Mikael Andersson,^g Michael Järvå,^h Rosmarie Friemann,^g Marco Piccinini,^b Cristina Ramondetti,^b Barbara Buccinnà,^b Salam Al-Karadaghi,ⁱ Donatella Boschi,^a Giuseppe Saglio^{e,f} and Marco L. Lolli^{*a}*

^a Department of Drug Science and Technology, University of Turin, 10125 Turin (Italy);

^b Department of Oncology, University of Turin, 10125 Turin (Italy);

^c Department of Molecular Biotechnology and Health Sciences, University of Turin, 10126 Turin (Italy);

^d Molecular Biotechnology Center, 10126 Turin (Italy);

^e Department of Clinical and Biological Sciences, University of Turin, 10043 Turin (Italy);

^f Mauriziano Hospital S.C.D.U. Hematology – 10128 Turin (Italy);

^g Department of Chemistry and Molecular Biology, University of Gothenburg, SE 405 Gothenburg (Sweden);

^h Department of Biochemistry and Genetics, La Trobe Institute for Molecular Science, La Trobe University, VIC 3086 Melbourne, Australia;

ⁱ Department of Biochemistry and Structural Biology, Lund University, 221 00 Lund (Sweden);

Keywords

Bioisosterism, dihydroorotate dehydrogenase (DHODH) inhibitors, leflunomide, brequinar, autoimmune diseases, hydroxyazoles, pyrazolo[1,5-*a*]pyridine, *acute myelogenous leukemia* (AML), myeloid differentiation.

Abstract

Human dihydroorotate dehydrogenase (*h*DHODH) catalyzes the rate-limiting step in *de novo* pyrimidine biosynthesis, the conversion of dihydroorotate to orotate. *h*DHODH has recently been found to be associated with *acute myelogenous leukemia*, a disease for which the standard of intensive care has not changed over decades. This work presents a novel class of *h*DHODH inhibitors, which are based on an unusual carboxylic group bioisostere 2-hydroxypyrazolo[1,5-*a*]pyridine, that has been designed starting from brequinar, one of the most potent *h*DHODH inhibitors. A combination of *structure-based* and *ligand-based* strategies produced compound **4**, which shows brequinar-like *h*DHODH potency *in vitro* and is superior in terms of cytotoxicity and immunosuppression. Compound **4** also restores myeloid differentiation in leukemia cell lines at concentrations that are one log digit lower than those achieved in experiments with brequinar. This paper reports the design, synthesis, SAR, X-ray crystallography, biological assays and physicochemical characterization of the new class of *h*DHODH inhibitors.

1. INTRODUCTION

Human dihydroorotate dehydrogenase (DHODH, EC 1.3.99.11) is a flavin-dependent enzyme located in the inner mitochondrial membrane and involved in the *de novo* pyrimidine biosynthesis. *h*DHODH is a therapeutic target that has been validated for the treatment of autoimmune diseases and cancer.¹⁻³ While a variety of *h*DHODH inhibitors have been studied over the years, leflunomide and its metabolite teriflunomide are still the only *h*DHODH-targeting drugs (Figure 1),⁴ approved for the treatment of rheumatoid arthritis and other autoimmune diseases.^{5,6} Brequinar, one of the most potent *h*DHODH inhibitors known to date, has been identified during the search for new compounds that would display clinical benefits similar to those of leflunomide, but without the associated side effects.⁷ Unfortunately, brequinar was discarded as a therapeutic agent when submitted to clinical trials for cancer,⁸ and for the prevention of organ transplant rejection,⁹ due to its severe side effects, a narrow therapeutic window and inconsistent pharmacokinetics.^{1,9,10}

In the fall of 2016, two publications,^{11,12} demonstrated the central role that *h*DHODH plays in *acute myelogenous leukemia* (AML), a disease for which standard intensive care has undergone little change over the last four decades.¹³ In AML, the most common acute leukemia in adults that affects the myeloid lineage of white blood cells, leukemic cells lose their ability to differentiate into adult white blood cells. This leads to the accumulation in the bone marrow of immature cells, which are characterized by high proliferation potential and known to interfere with the production of normal blood cells. The disease progresses rapidly and is typically fatal within weeks or months if left untreated. A study by Sykes et al.,¹¹ suggested that *h*DHODH plays a central role in the regulation of myeloid differentiation in both *in vitro* and *in vivo* models, and thus opens up totally new perspectives for AML treatment. Using brequinar, the authors showed that *h*DHODH inhibition has a profound effect on the induction of myeloid differentiation, delay of disease development and

reduction of the burden of leukemia-initiating cells in various AML mouse models, human cell line xenografts, patient-derived xenografts and syngeneic mouse models.

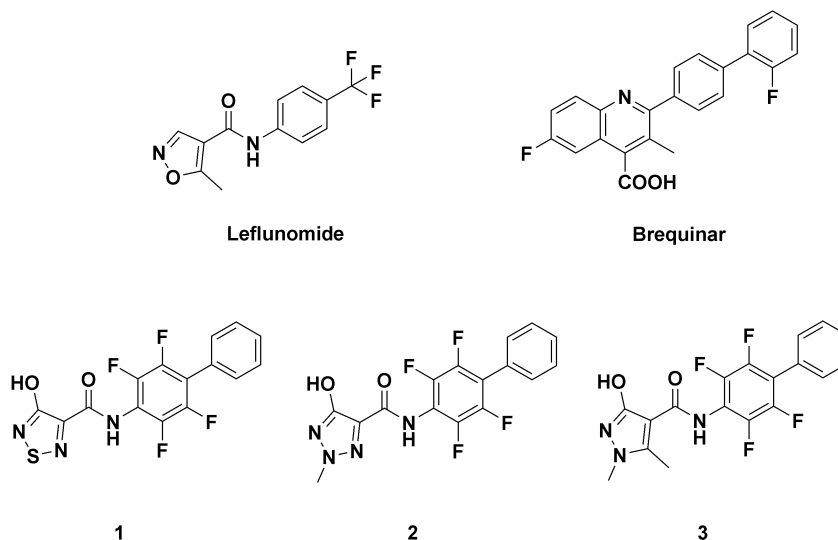


Figure 1. *Leflunomide*, *brequinar* and hydroxyazole analogues **1** – **3**.¹⁴

The discovery of the central role of *h*DHODH in AML immediately attracted the interest of the pharmaceutical industry. Two newly-patented *h*DHODH inhibitors are currently being investigated for the treatment of AML. The first one, ASLAN003 (by ASLAN Pharmaceuticals), entered Phase II clinical trials in November 2017 (NCT03451084), while the second compound by Bayer (BAY2402234), entered Phase I clinical trials in January 2018 (NCT03404726). In May 2018, the patent containing the BAY2402234 structure and a description of the activity profile has been published.¹⁵

The large number of new *h*DHODH inhibitors that have been reported in recent years,^{2, 4 16-19} and the rising interest from the industry suggest that there is a wide interest towards the development of new *h*DHODH inhibitors.

We have recently introduced a new generation of *h*DHODH inhibitors^{14, 20} that were designed via scaffold-hopping replacement of brequinar's acidic moiety with a variety of acidic hydroxylated azoles.^{14, 20-24} Three of these compounds (**1**, **2** and **3**), which are based on hydroxythiadiazole, hydroxytriazole and hydroxypyrazole respectively (Figure 1), showed high *h*DHODH inhibitory activity *in vitro*, with compound **1** being the best in the series with

an IC_{50} value of 16 nM. The X-ray crystallographic structures of **1**, **2** and **3** in complex with *h*DHODH showed that the acidic scaffolds of the compounds interact with Arg136 at subsite 2 of *h*DHODH ubiquinone binding site,¹⁴ in a way reminiscent of the interactions formed by the carboxylic group of brequinar.²⁵ In addition, each scaffold was able to establish interactions with the small lipophilic pocket created by Val143 and Val134, known as subsite 4 (the location of the subsites is shown by numbers in Figure 3). When assessed for antiproliferative activity, the compounds were found to be effective in the same concentration range as brequinar, although with much lower cytotoxicity, showing cytotoxic effects first at 70-times the concentrations required to inhibit cell proliferation.

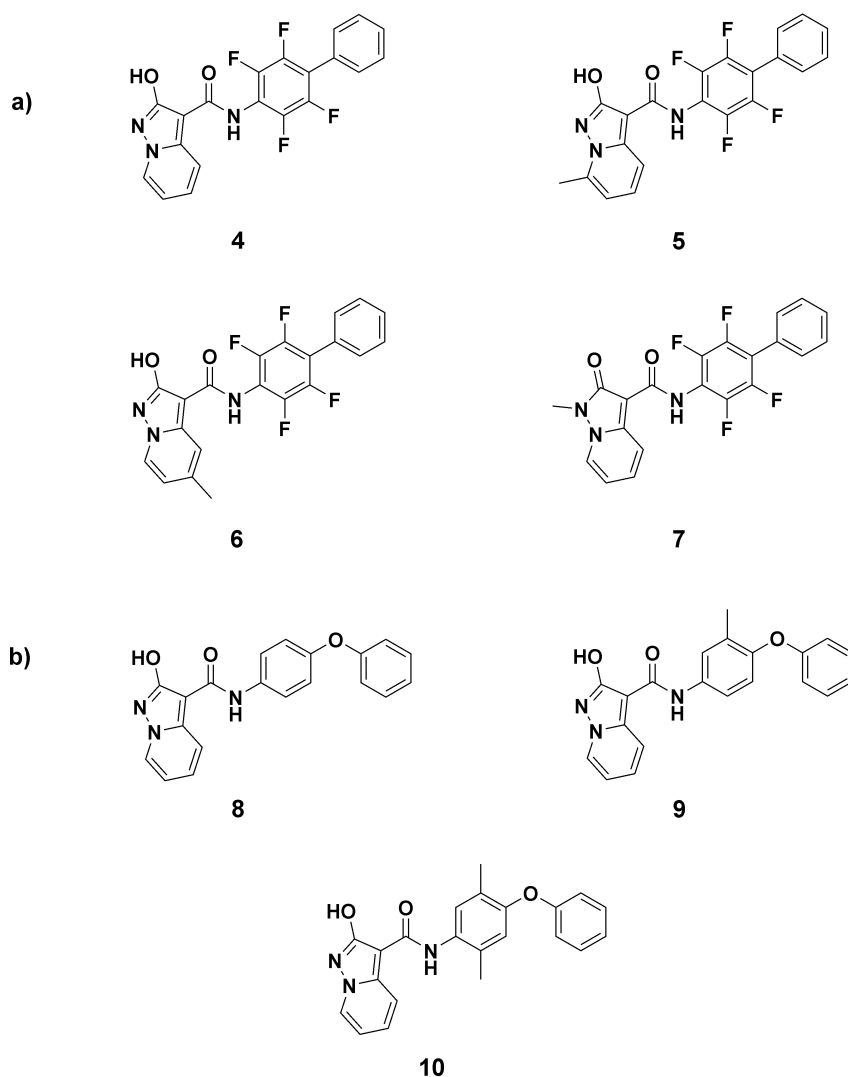


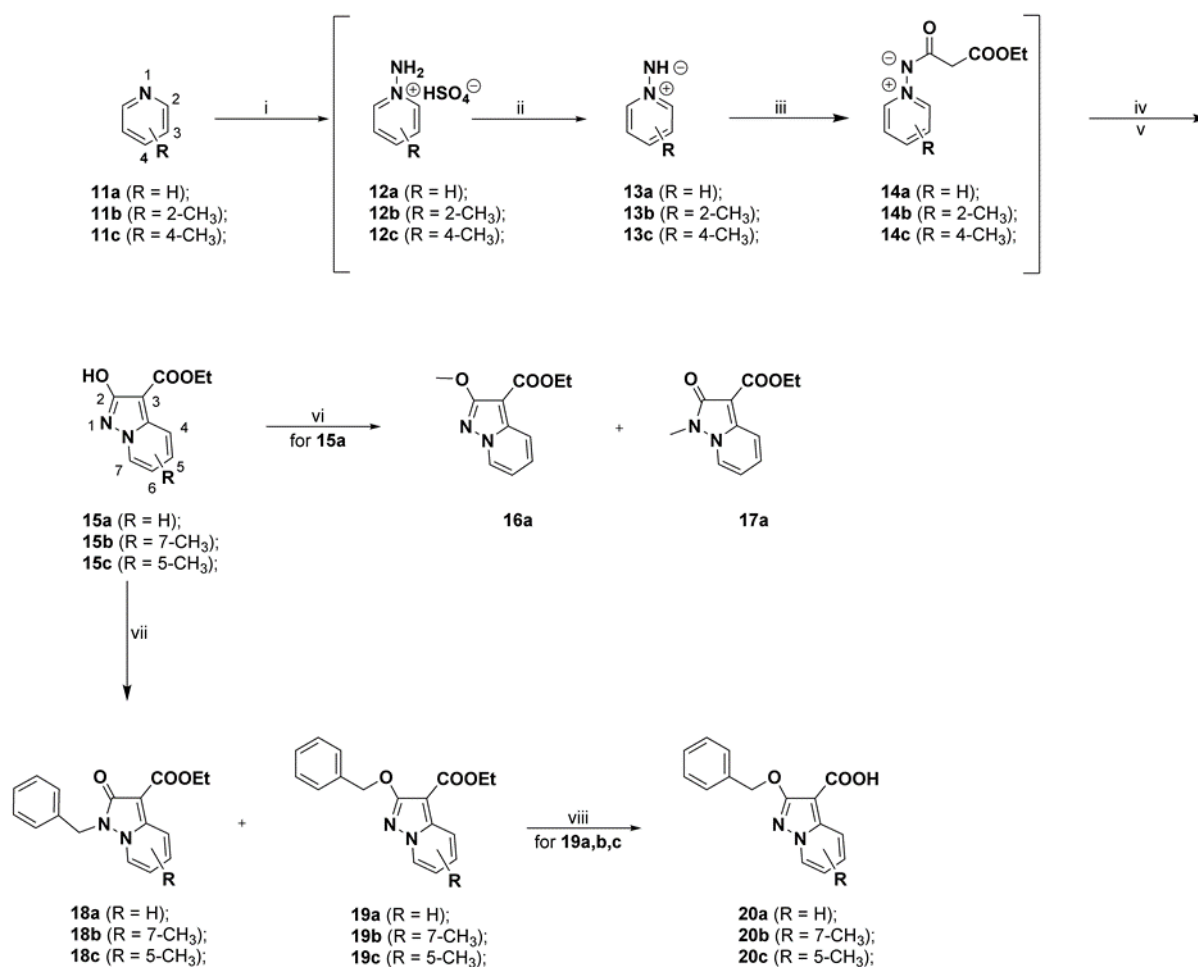
Figure 2. Structures of compounds **4** – **10**, which are based on the 2-hydroxypyrazolo[1,5-*a*]pyridine scaffold and characterized by the presence of either a biphenylic (a), or biphenyl ether substituent (b).

This work reports the design of a new series of potent *h*DHODH inhibitors based on 2-hydroxypyrazolo[1,5-*a*]pyridine as an acidic scaffold, a system that is still relatively unexplored in the literature. Here we report the first scaffold-hopping study of this structure aimed at generating a bioisostere with a carboxylic function. In the first series, besides investigating the moiety itself (compound **4** and **7**, Figure 2a), we have also investigated the effect of introducing a methyl group into the pyridine ring in order to improve its lipophilic interaction with subsite 4 (compounds **5** and **6**, Figure 2a). In the second series (compounds **8** - **10**, Figure 2b), we replaced the biphenyl substituent with a more flexible and polar diphenyl ether in order to improve pharmacokinetics and provide more drug-like properties.²⁶ This paper reports and discusses the design principles, modeling, synthesis, SAR and X-ray crystallographic analysis of this new generation of *h*DHODH inhibitors. In addition, biological assays (including cell viability, proliferation, cytotoxicity, immunosuppression and myeloid differentiation), physico-chemical characterization and preliminary drug-like properties are also presented.

2. RESULTS AND DISCUSSION

2.1 Chemistry: synthesis of target compounds **4** – **10**.

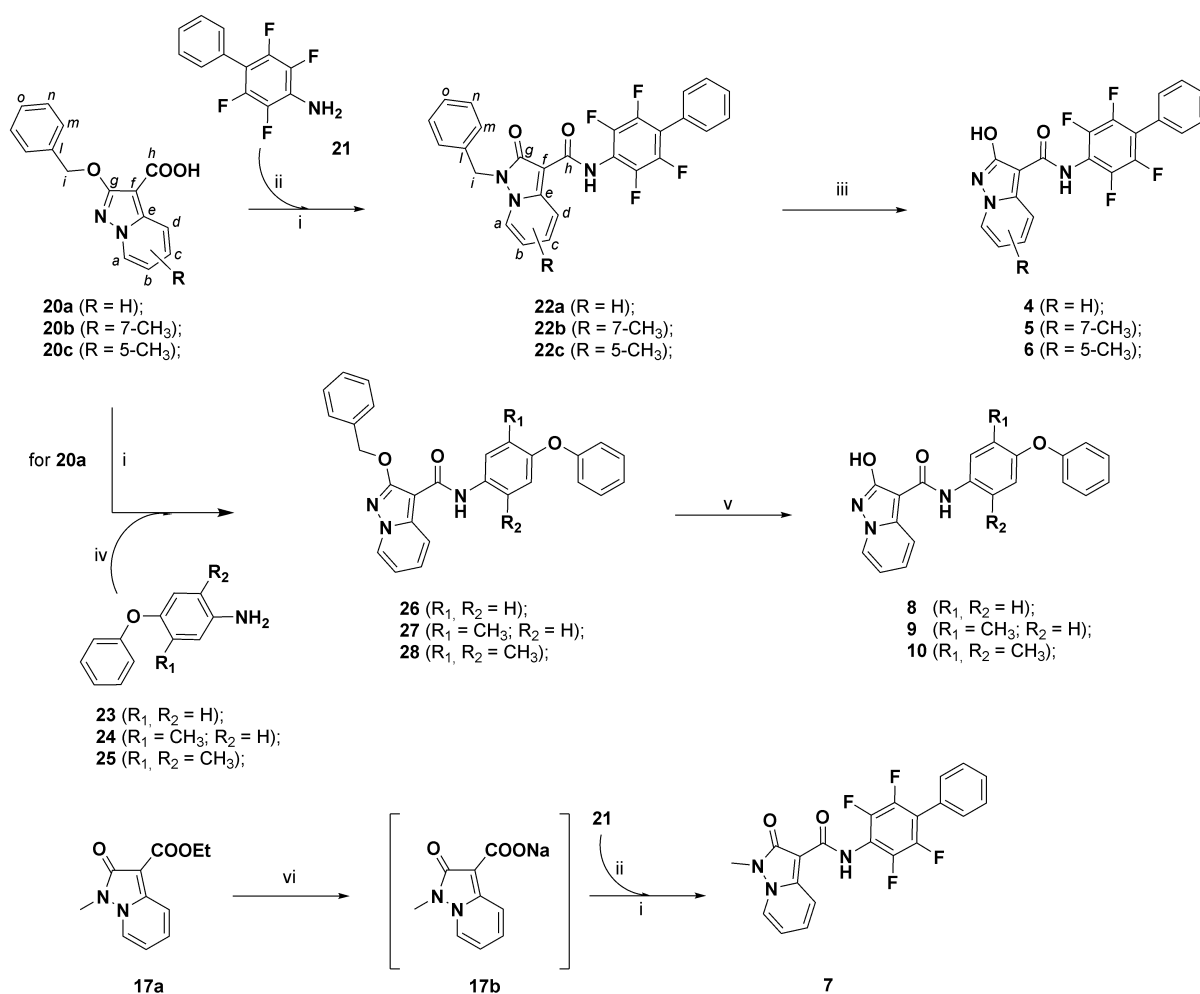
The chemical strategies used to produce **17a** and the regiosubstituted, protected 2-hydroxypyrazolo[1,5-*a*]pyridine building blocks **20a-c**, which are useful in the syntheses of target compounds **4** - **10**, are shown in scheme 1.



Scheme 1. Synthetic strategies for the preparation of substituted hydroxylated pyrazolo[1,5-a]pyridine intermediates. i) HOSA, H₂O, 90 °C; ii) K₂CO₃, EtOH; iii) diethylmalonate, ethanol, 90 °C; iv) *t*-BuO⁻K⁺, dry THF v) 0.1 N HCl; vi) Cs₂CO₃, MeI, dry THF, 40 °C; vii) Cs₂CO₃, BnBr, dry DMF, viii) 5 M NaOH, ethanol, 70°C.

Compounds **15a,b,c** were prepared via a slight modification to a known procedure (Scheme 1),²⁷ starting from either pyridine or the corresponding substituted pyridines. Compounds **12a - c** were obtained by aminating the substituted pyridines **11a - c**, using hydroxylamine-O-sulfonic acid (HOSA) as the aminating reagent. The products were treated with K₂CO₃ to give the yields of **13** that were reacted with diethyl malonate in EtOH to give intermediate types **14**, which were, in turn, converted into the desired compounds **15a - c**, in the presence of a strong base (*t*-BuO⁻K⁺), with 18 – 21 % overall yields.

Although some examples have been reported in the literature,²⁸ the reactivity pattern that 2-hydroxypyrazolo[1,5-a]pyridines show towards alkylating agents has never been fully investigated. Both O- and N- alkylation patterns must always be considered,^{14, 29} when considering the reactivity of substituted hydroxylated azoles. The type of the heteroatom within the heterocyclic system and the choice of the alkylating agent used usually control the alkylation pattern.^{14, 23, 30} Moving onwards in Scheme 1, the alkylation of **15a - c** with benzyl bromide also gave the corresponding N-alkylated derivatives **18a - c** (ratio 5 – 29 %), besides desired O-alkylated compounds **19a - c**, in each case. A similar result was obtained when methyl iodide was used as an alkylating agent on **15a**, producing the methylated isomers **16a** and **17a** in 35 % and 59 % yields, respectively. 2D-NMR spectroscopy was used to univocally attribute the relative isomeric structures (see Supplementary material). Esters **19a - c** were then hydrolyzed under basic conditions to obtain the corresponding acids **20a - c** in good yields, which were then used for the preparation of targets **4 – 6, 8 - 10**, as described in scheme 2.



Scheme 2. Synthesis of targets **4 - 10**: i) oxalyl chloride, dry DMF, dry THF; ii) AlMe₃, dry toluene, reflux; iii) H₂, Pd/C, 37 % HCl, ethanol; iv) dry toluene, reflux; v) H₂, Pd/C, dry THF, vi) 5M NaOH, ethanol, r.t.

Starting from acids **20a - c** (see Scheme 1), the corresponding acyl chlorides were obtained via treatment with oxalyl chloride in dichloromethane and used directly after drying without any further purification. In order to improve their reactivity with acyl chlorides, 2,3,5,6-tetrafluoro-4-phenylaniline (**21**), was converted into its corresponding dimethylaluminum amide. The desired amides **22a - c** were obtained in the 38 - 45 % yield range. Interestingly, the benzylic protection transposed from the exocyclic oxygen to the endocyclic N1 nitrogen during coupling (see Supplementary for the characterization details. The ¹³C-NMR chemical shifts of the CH₂ benzylic nucleus were diagnostic for the structural attribution of N-benzyl or O-benzyl derivatives of **22a - c** and **26 - 28** respectively as for compounds **18a** and **19a**).

On the other hand, the coupling of the acyl chloride, derived from **20a**, with phenoxy anilines **23 - 25** produced the expected O-benzyl-protected amides **26 - 28**, as desired. This difference in reactivity led us to correlate the migration of the benzyl group with the presence of a Lewis acid in the reaction mixture. Compounds **22a - c** and **26 - 28** were then converted to the desired target compounds **4 - 6, 8 - 10** by applying room-pressure catalytic hydrogenation conditions. The same approach was applied to the preparation of **7**. In this case, the acidic compound obtained from the hydrolysis of **17b** was quite unstable, meaning that any isolation attempt resulted in decarboxylation. We avoided this decomposition by isolating the intermediate as a sodium salt and transforming it into the corresponding acyl chloride. The acyl chloride was stable enough to react with the dimethylaluminum amide of 2,3,5,6-tetrafluoro-4-phenylaniline producing compound **7** with a 27 % yield.

2.2 Inhibition of *h*DHODH and structure-activity relationships (SAR).

Initially, we evaluated recombinant *h*DHODH inhibition activity of compounds **4 - 10** using brequinar, teriflunomide and the hydroxytriazole analogues **2**,¹⁴ as reference compounds (Table 1). Among the first-generation compounds **1 – 3**, compound **2** showed the best balance between *h*DHODH potency and cell cytotoxicity and, for this reason, it was considered to be the most promising compound and included in this study as reference.

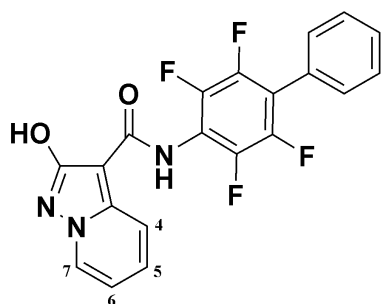
Compound	<i>h</i> DHODH ^a IC ₅₀ ± SE (μM)	Proliferation ^b IC ₅₀ ± SE (μM)	Proliferation ^b IC ₅₀ ± SE (μM) + Uridine	Cytotoxicity ^c (effect ≥ 30%) (μM)	Immuno- suppression ^d IC ₅₀ ± SE (μM)	Immuno- suppression ^d IC ₅₀ ± SE (μM) + Uridine
Brequinar	0.0018±0.0003	0.91±0.07	94.17±2.08	48.2±0.8	3.74±0.06	59.64±2.18
Teriflunomide	0.388±0.064	43.22±1.24	nd	53±3	54.3±3.1 ¹⁴	nd
2	0.045±0.013	1.88±0.06	nd	>100	8.9±0.7 ¹⁴	nd
4	0.0012 ± 0.0002	0.75±0.04	68.69±2.35	60.4±1.2	0.78±0.06	57.15±2.06
5	0.0043±0.0005	0.82±0.03	35.62±0.98	41.3±1.5	0.77±0.08	46.84±1.27
6	0.035 ± 0.003	1.56±0.08	88.45±1.48	48.6±2.3	1.08±0.10	52.39±1.46
7	> 5	nd	nd	nd	nd	nd
8	0.760 ± 0.136	89.66±1.64	95.63±2.11	>100	69.25±2.47	>100
9	0.480 ± 0.031	67.55±1.21	>100	>100	35.26±2.34	>100
10	0.043 ± 0.005	1.47±0.06	55.13±2.05	>100	0.84±0.16	74.69±1.63

Table 1: Biological effects of compounds **2**, **4** – **10**, brequinar and teriflunomide. The effect of the compounds (expressed as IC₅₀ value, except for cytotoxicity), on ^a *h*DHODH *in vitro* assay; ^b cell proliferation inhibition (Jurkat T cells); ^c cytotoxicity, concentration of compounds causing a significant (≥ 30%) cytotoxic effect (Jurkat T cells); ^d PHA-stimulated PBMC proliferation inhibition. The “nd” notation indicates that the compound was not tested in that specific assay.

2-Hydroxypyrazolo[1,5-a]pyridine analogue **4** (IC₅₀ = 1.2 nM), was found to be the most potent inhibitor in the series, as it had 320 times higher activity when compared to teriflunomide (IC₅₀ = 388 nM), and comparable activity to brequinar (IC₅₀ = 1.8 nM) in the enzymatic assay. A crystallographic study (see section 2.3) was carried out to experimentally determine the binding pose of compound **4** in the ubiquinone binding pocket of *h*DHODH. It is interesting to note here how brequinar-like potency was obtained even when a weaker acidic moiety (a table containing the p*K*_a values of hydroxyl-pyrazolo[1,5-a]pyridine

analogues is included in the Supplementary section, see Table S2), was involved in the key interaction with Arg136 at subsite 2. Moreover, this interaction is essential for activity, as the neutral compound **7** is totally inactive.

Further, we focused on the possibility of decorating the “pyridine” part of compound **4**, to add an interaction with the small lipophilic pocket created by Val134 and Val143 at subsite 4. Here, we carried out relative binding free-energy calculations (i.e., the relative difference in binding energy between two compounds) using a non-physical thermodynamic cycle. The differences in binding affinities for the protein-ligand complexes were calculated with the aid of free-energy perturbation (FEP) approach based on Molecular Dynamics (MD) simulations, the methodological detail are given in the supplementary information.³¹ The four available positions of **4**, indicated in Table 2, were explored using MD/FEP methyl and chlorine scans to identify the most promising sites for a beneficial hydrogen substitution.^{32, 33}



	H to Cl $\Delta\Delta G$ (kcal/mol)	H to CH ₃ $\Delta\Delta G$ (kcal/mol)
C4	-0.35 \pm 0.02	1.49 \pm 0.07
C5	-0.48 \pm 0.02	1.19 \pm 0.07
C6	0.87 \pm 0.02	2.59 \pm 0.07
C7	-1.43 \pm 0.02	0.15 \pm 0.09

Table 2. MD/FEP results of the change in calculated free energy of binding (in kcal/mol), and the computed uncertainty, for the introduction of chlorine and methyl substituents on the 2-hydroxypyrazolo[1,5-a]pyridine motif of compound **4**.

The calculated $\Delta\Delta G$ values indicate that the chlorine group is generally preferred over the methyl in all the positions, since negative values represent higher binding affinity. Among the four sites, position 7 is the most energetically profitable for a substitution as it is

associated with the lower energy value of -1.43 for the chlorine and has only a marginal effect on the energy in the case of the methyl group (0.15). Replacement of the hydrogen in position 6 is less favorable as it is evident from the higher positive energy values for the chlorine (0.87) and the methyl (2.59). Positions 4 and 5 show comparable behavior, with substitution in 5 only slightly better tolerated than in 4 for both groups.

A probable reason of a better tolerability of the chlorine substitution as compared to the methyl group could be a result of the interaction of the 2-hydroxypyrazolo[1,5-a]pyridine moiety with the side chain of His56 (see section 2.3). Here, the π -stacking interaction energy of the aromatic rings could be complemented by the electron-withdrawing effect of the additional chlorine in compound **4**.³⁴ The FEP results also show that methyl modulations did not lead to an improvement in $\Delta\Delta G$, suggesting that additional lipophilic interactions did not contribute to the binding affinity. This also supports the importance of the electrostatic effects of the substituents on the interactions. Remarkably, similar variations of $\Delta\Delta G$ were found among the four positions for both methyl and chlorine scans. It was also noted that the most tolerated position for substituents was at C7 (Table 2) - it appears that small groups at this position could make use of the space created around Val143, Val134 and Arg136. On the other hand, the predicted changes in the free energy revealed that replacements at C6 do not provide any advantages, presumably due to the steric effects associated with the side chains of Val134 and Val143. FEP analysis on C4 and C5 showed comparable results, suggesting that the placement of additional lipophilic groups at subsite 3 of the enzyme did not contribute to any new favorable interactions.

Moving to experimental assessment and taking into account the MD/FEP results, the two most tolerated positions 5 and 7 were considered in the next investigations. Since the chlorine derivatives of **4** are not currently synthetically accessible, compounds with methyl substituents in positions 7 and 5 were synthesized (Scheme 1), leading to compounds **5** and **6**, respectively. While the substitution at position 5 decreased the activity 29 fold (**6**, $IC_{50} = 35$

nM), as compared to compound **4**, the substitution at position 7 yielded a similar profile (**5**, $IC_{50} = 4.3$ nM).

In the second series (compounds **8** - **10**, Figure 2), the replacement of the biphenylic substituent was investigated in an attempt to improve pharmacokinetics and obtain more drug-like compounds.²⁶ In our earlier studies,^{14, 20} optimal interactions with the lipophilic subsite 1 were only guaranteed with a tetrafluoro substitution on the first ring. Conformational analyses,³⁵ underlined the role of incremental fluorine substitution on the first ring in stabilizing the brequinar-like binding mode, which has previously been found to be connected with higher inhibitory potency.²⁵ For example, the removal of two or three fluorine atoms from the biphenylic scaffold of triazole analogue **2** resulted in a dramatic drop in inhibitory activity.¹⁴ However, the presence of the tetrafluorobiphenylic substituent is detrimental for the solubility of the derivatives.²⁶ We therefore decided to design analogues that lacked a biphenylic scaffold in order to explore novel possibilities. Inspiration was taken from a recent study by Das *et al.*,³⁶ in which brequinar-like activity was replicated by a brequinar-related compound that included a substituted diphenylether; compounds **8** – **10**, which contain a variety of diphenylether substituents, were thus designed. Although a dramatic drop in activity was observed in moving from **4** ($IC_{50} = 1.2$ nM) to **8** ($IC_{50} = 760$ nM), compound **8** firstly proved the possibility to design inhibitors where the biphenylic is replaced by the diphenylether scaffold. The addition of a methyl group at position 3 of the first ring (compound **9**), led to activity moving closer to the teriflunomide range ($IC_{50} = 480$ nM). Adding a second methyl at position 6 (compound **10**), finally allowed a nM range to be reached ($IC_{50} = 43$ nM). On the basis of these results, we envision that the increased rigidity granted by the double methyl substitution and the increase in hydrophobicity might be crucial for activity.

2.3 Binding mode analysis: crystallographic and molecular modeling studies.

In order to achieve further insights into the binding mode of this new generation of 2-hydroxypyrazolo[1,5-a]pyridine moiety-based inhibitors, we determined the crystal structure of the complex between **4**, as it is one of the most potent *h*DHODH inhibitors yet described, with the protein. The crystals diffracted to 1.58 Å (PDB id: 6FMD) and the structure was determined by molecular replacement. X-ray data and refinement statistics are summarized in Table S1 (Supplementary). The inhibitor was clearly bound in the ubiquinone binding site with high quality electron density (see Supplementary. Figure S2). It shows a binding mode that can be perfectly superimposed onto the previously reported crystal structure of the complex with brequinar (Figure. 3).¹⁴ As can be seen in Figure 3, which shows the entrance of the binding pocket, the tetrafluorobiphenilic moiety of compound **4** is positioned in subsite 1, a lipophilic cavity that is built up by Met43, Leu42, Leu46, Ala59, Phe62, Phe98 Leu68, Leu359 and Pro364. The hydroxyl-pyrazolo[1,5-a]pyridine moiety is extended over subsites 2 and 3, occupying the innermost part of the pocket. In addition, there is an ion bridge extending to the side chain of Arg136 and a hydrogen bond with the side chain of Gln47. The pyridine moiety is seen to be able to fit perfectly within the lipophilic subsite 4 (Val134 and Val143). As this interaction is the only difference between this and the previous generation of inhibitors, it appears to be the reason for compound **4**'s high potency, which is more than 10 times that of our best earlier generation compound,¹⁴ the thiadiazole **1** (IC₅₀ 16 nM).

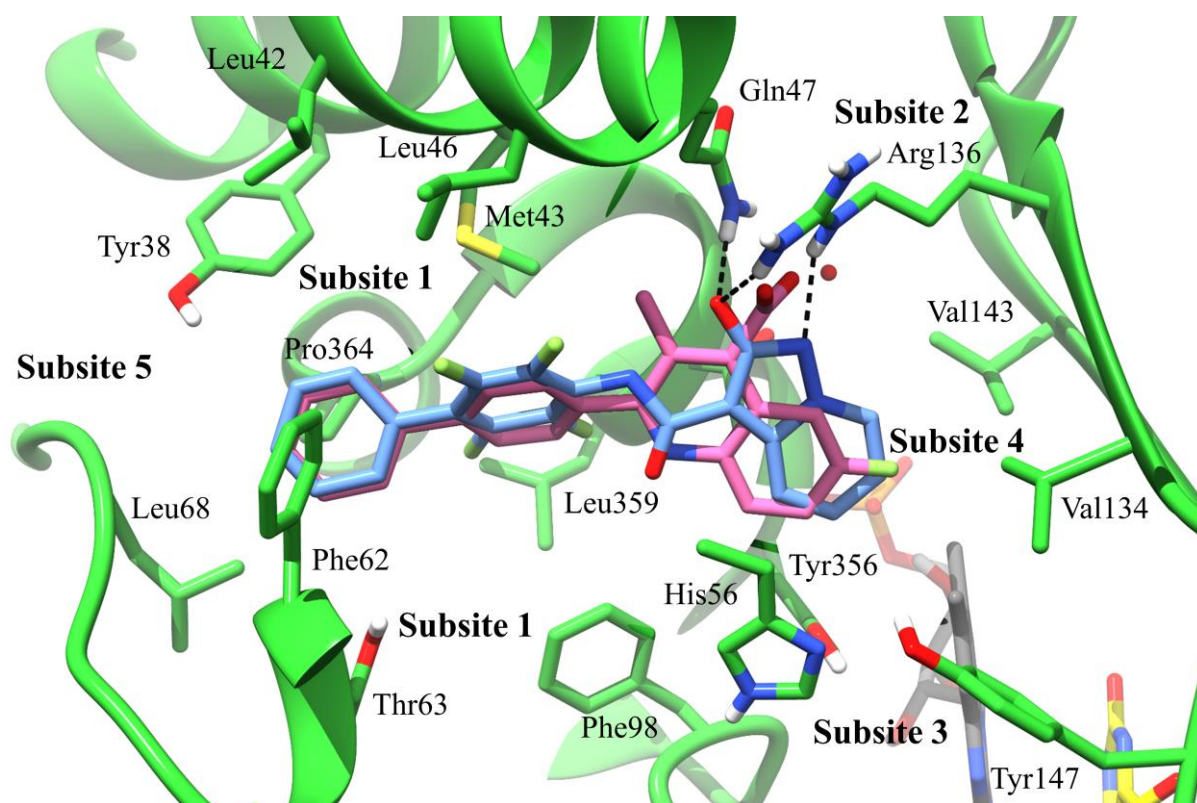


Figure 3. Ubiquinone binding sites of *h*DHODH co-crystallized with compound **4** (blue) (PDB id: 6FMD), superimposed on the complex with brequinar analog, (PDB id: 1D3G); only the ligand is shown in pink. Hydrogen bonds are shown as dashed lines. Flavin mononucleotide and orotate are represented in grey and yellow, respectively.

Compound **10** represents a good starting point for future modulation of the small diphenylether series (**8** – **10**). Its activity towards *h*DHODH is just comparable to that observed for triazole **2**, which is one of the best compounds in the first series. In order to better understand the role played by substitutions at the first diphenylether ring in influencing activity, a MD study was performed on compounds **4**, **8**, **9** and **10**. Starting from the docked conformation of the four compounds in the target binding site, 50 ns long MD simulation for each compound was carried out. The root mean square deviations (RMSD) for the ligands and the protein α carbon chain were calculated with respect to the starting structures. In each system analyzed, the protein structures reached stability after a few ns of simulation and then remained stable with an RMSD of around 0.95 Å (Figure S1). More interesting still is the

change in RMSD of the atomic coordinates of the ligands in the binding site. Figure 4 shows the average conformations of compounds **4**, **8**, **9**, **10** assumed during the MD simulations and the relative RMSD plots.

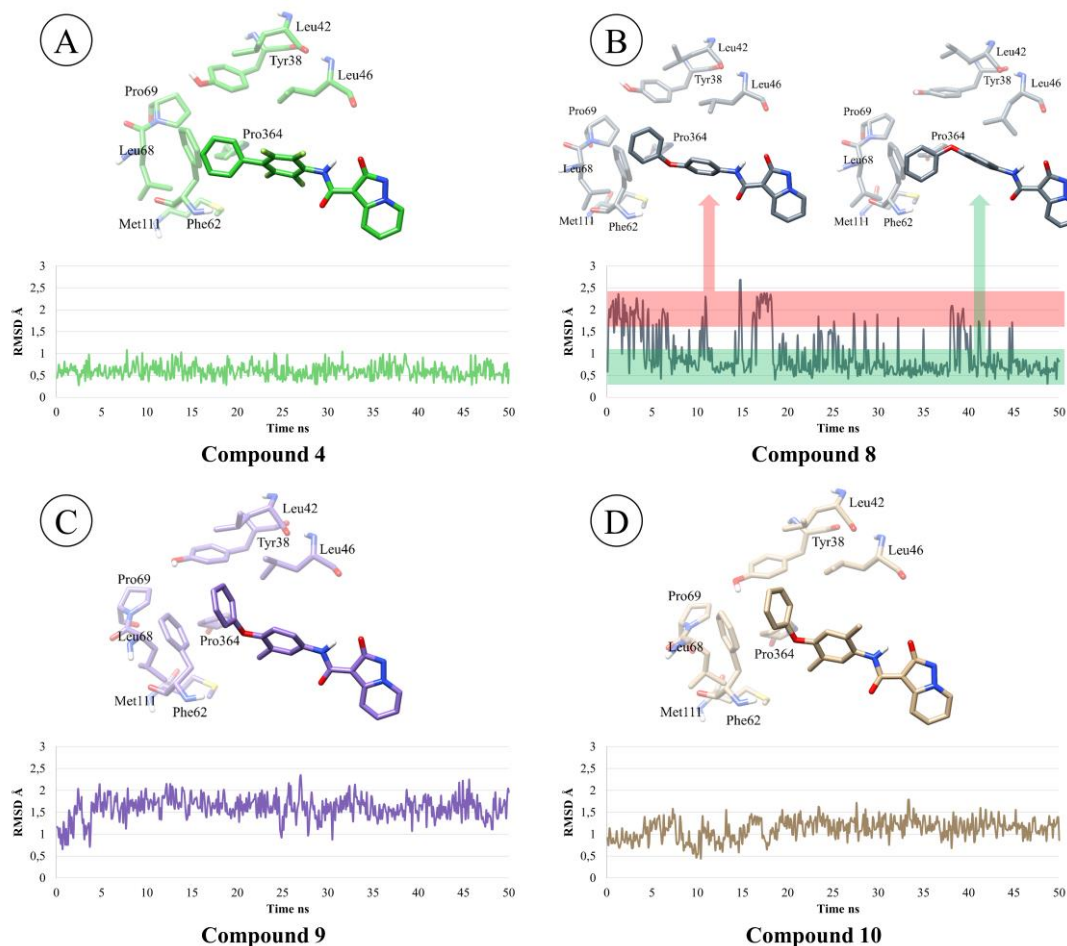


Figure 4: The graphs show the evolution of the RMSD values (calculated for ligand heavy atoms as compared with starting structures) of the *h*DHODH complex analyzed by MD simulation. A, B, C and D in the figure correspond to compounds **4**, **8**, **9**, **10**, respectively. The compounds and surrounding amino acids are in the average conformations assumed during MD simulations.

While compound **4** shows a stable conformation, with an average RMSD of around 0.6 Å (Figure 4A), in all the other simulations considerably higher RMSD values were obtained for compound **8** (Figure 4B). The unsubstituted first ring in compound **8** allows free rotation of

the phenyl-O-phenyl dihedral angle inside subsite 1, leading to the conformational variability seen along the MD trajectories. During the simulation, as seen in Figure 4B, compound **8** appears to have two relatively stable conformations in which one is similar to the starting docking pose, identified by an RMSD of around 0.6 Å. In the second, the distal phenyl of the diphenylether points towards Tyr38, leading to an RMSD of around 2.0 Å. As long as activity values are concerned, the alternating behavior observed for compound **8** results in a loss of an interaction, which is reflected in reduced activity. Substitution on the first ring in compounds **9** and **10** (Figure 4C and 4D), led to a more stable profile. In fact, after an initial increase in RMSD, the compounds reached a steady conformation with average RMSDs of around 1.6 and 1.2 Å, respectively. Activity values appear to indicate that the additional degree of freedom associated with the diphenylether is strictly correlated with the compounds' binding affinity. Indeed, the introduction of methyl substituents in compounds **9** and **10** seems to stabilize the favored binding conformations leading to a more optimal interaction with the protein. It is worth noting that the activity of compound **9**, which is only slightly higher than that of **8**, clearly indicates how a single substitution is not sufficient to achieve the rigidity required for optimal binding affinity. On the other hand, the double methyl substitution in compound **10** is able to recover the activity, which reaches a nM range, suggesting that molecule rigidity is one of the key attributes for *h*DHODH structure-activity relationship (SAR).

Although MD analysis gives important insights into the role of the diphenylether moiety in the binding to *h*DHODH, the free energy of binding (FEB) was still required for the understanding of the structure-activity relationships. MM/GBSA calculations were used to provide a quantitative way to evaluate the different components of interaction energy that contributes to binding of compounds **4**, **8**, **9** and **10**. All the free energies were computed on the last 40 ns of the simulated trajectory. Detailed results are summarized in Table 3.

Ligand	IC ₅₀ (nM)	ΔTotal^a	ΔE_{vdW}^b	ΔE_{elec}^c	$\Delta E_{\text{elec.solv}}^d$	ΔG_{gas}^e	ΔG_{solv}^f
4	1.2	-40.87	-55.44	-57.57	78.91	-113.02	72.14
8	760	-36.08	-53.80	-62.28	86.46	-116.08	80.00
9	480	-37.18	-53.80	-60.92	84.09	-114.72	77.54
10	43	-40.32	-56.68	-63.42	86.55	-120.09	79.77

Table 3. Free energy analysis for the binding of compounds **4**, **8**, **9** and **10** to *h*DHODH. ^{a)} Final estimated binding free energy calculated from the terms below. ^{b)} Nonbonded van der Waals. ^{c)} Nonbonded electrostatics. ^{d)} Electrostatics contribution to solvation. ^{e)} Total gas phase energy. ^{f)} Sum of nonpolar and polar contributions to solvation.

The MM-GBSA calculations show a good agreement with the experimental activity data. According to the experiments, the difference in FEB of compound **4** ($\Delta\text{Total} = -40.87$ kcal/mol) and **8** ($\Delta\text{Total} = -36.08$ kcal/mol) is found more than 4 kcal/mol, suggesting that **4** is the most active in the series. Moving to compounds **9** ($\Delta\text{Total} = -37.18$ kcal/mol) and **10** ($\Delta\text{Total} = -40.32$ kcal/mol), obtained by modulation of the first ring of compound **8**, an improvement of the ΔTotal can be observed. While the computed free binding energy for compound **9** is still close to **8**, compound **10** shows a free energy value close to **4**. Detailing the binding free energy composition, it can be noticed how electrostatic components contribute more in **8**, **9** and **10**, if compared with **4**. On the other hand, electrostatic solvation ($\Delta E_{\text{ele,solv}}$) disfavors the binding of the diphenylether series because of a greater de-solvation penalty respect the tetrafluorinated biphenyl scaffold. Remarkably, considering the van der Waals contributes (ΔE_{vdW}), only **10** reaches a value that overcome compound **4**. A per-residue energy decomposition (PRED) analysis was also performed in order to identify the key residues that contribute to binding affinity at the binding site.

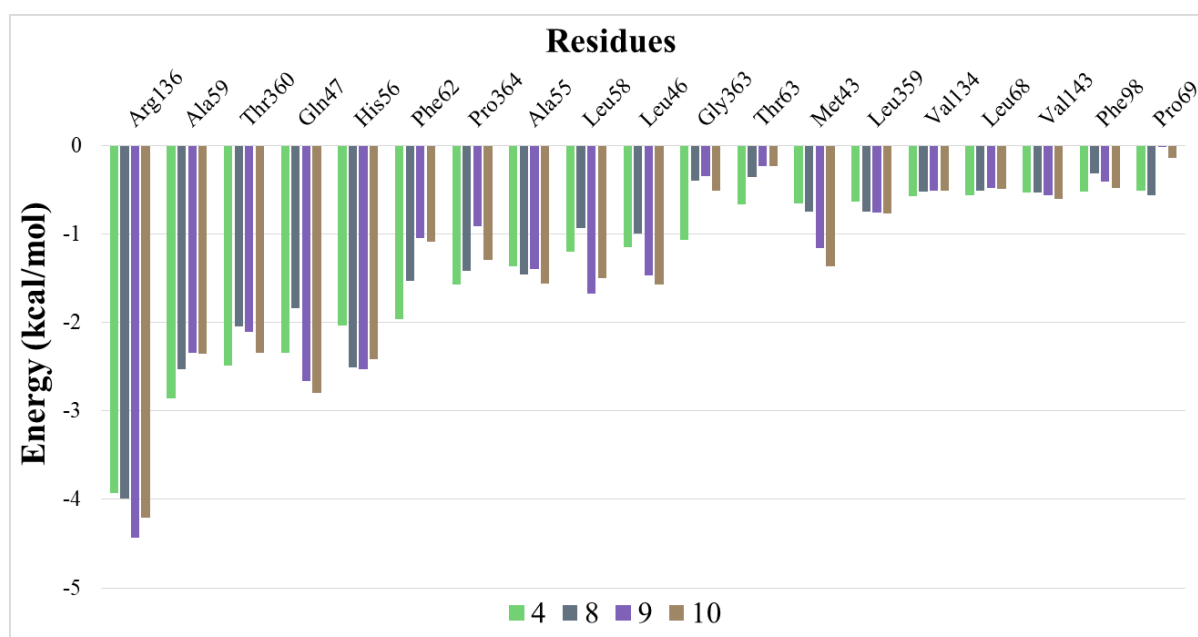


Figure 5. The per-residue free energy contribution to binding for compounds **4**, **8**, **9**, **10**.

As shown in Figure 5, Arg136 and Glu47 mainly contribute to binding, pointing to the significance of the interactions with these residues. PRED results are consistent with the binding mode proposed for compound **9** (data not shown), and **10** (Figure 6). For Met43, Leu46 and Leu58, the energy contributions suggest a higher interaction with **9** and **10** respect compound **4**. This result is in agreement with the observed slightly different position assumed by **10** at binding side if compared with **4**. Moreover, per-residue free energy analysis also suggest that Phe62 is a key residue for binding. On the basis of X-ray structure (Figure 6), the side chain of Phe62 is involved in a π - π interaction with the distal phenyl of **4**. The binding contribution of Phe62 for **9** and **10** (-1.05 kcal/mol and -1.09 kcal/mol, respectively) is less than about 1 kcal/mol compared to **4** (-1.97 kcal/mol). This is according to binding mode of **10**, where the staking interaction with Phe62 is partially lost because the shifting of the second ring of the diphenylether toward the cavity composed by Leu42, Leu46 and Tyr38.

Taken together, MD and FBE analysis are coherently with bioassay results and explain the SAR of replacement on diphenylether scaffold, highlighting how methyl groups on the first

ring gave an important contribute to stabilize the bioactive conformation by decreasing ligand flexibility and optimizing the interactions with subsite 1 and 2.

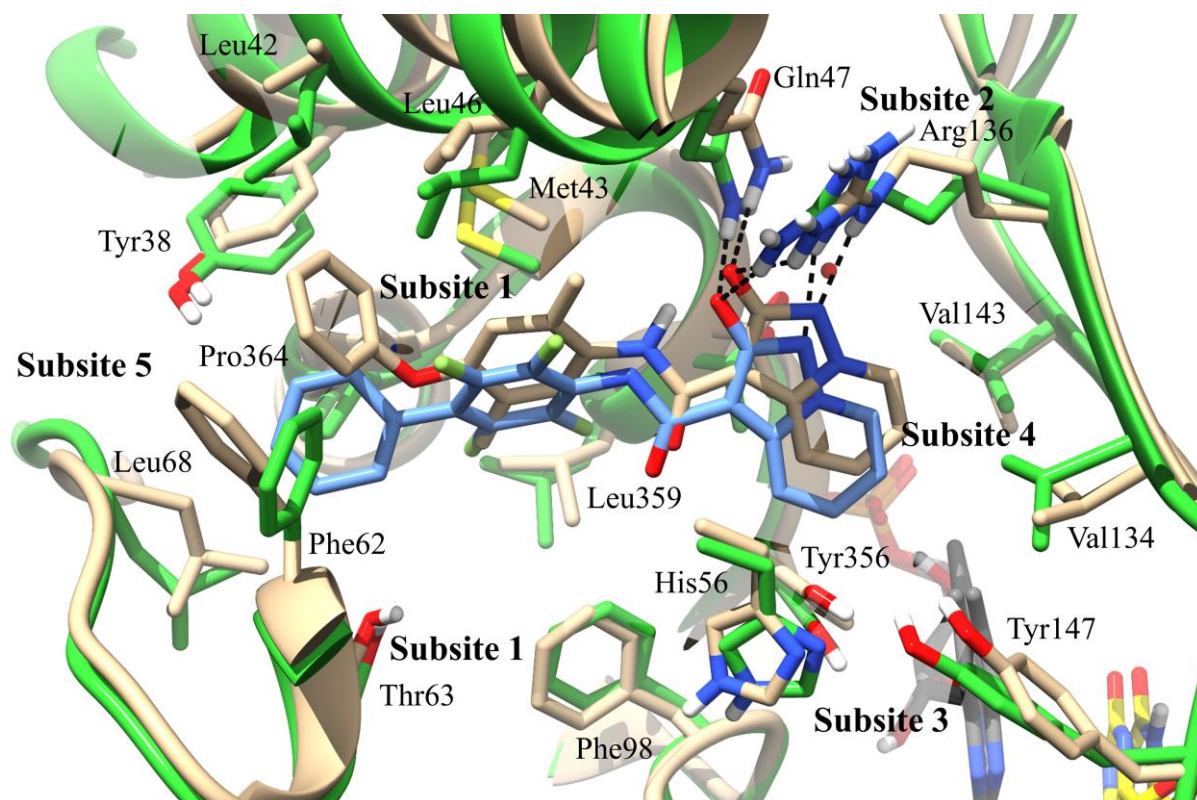


Figure 6. Ubiquinone binding sites of *hDHODH* with bound compound **4** (PDB id: 6FMD, protein in green and ligand in blue), superimposed on the average structure of the *hDHODH*-compound **10** complex produced in MD simulation (protein and ligand in tan). Hydrogen bonds are shown as dashed line. Flavin mononucleotide and orotate are represented in grey and yellow, respectively.

2.4 Cell based assays.

2.4.1 Proliferation, cytotoxicity and immunosuppression on Jurkat cells.

After evaluating compounds **4** - **10** for their ability to inhibit recombinant *h*DHODH *in vitro*, active compounds **4** - **6** and **8** - **10** were tested for their effects on cell proliferation in Jurkat T cells (Table 1). The stability of the compounds under the applied experimental conditions was also checked and they were all found to be stable (See Supplementary). The potent *h*DHODH *in vitro* activity observed for compounds **4** and **5** was translated into a potent antiproliferative effect, which was slightly superior to that of brequinar itself in both cases. Compounds **6** and **8** - **10** displayed similar profiles, although weaker *h*DHODH potency was reflected in weaker antiproliferative effects. Besides **4** and **5**, **6** and **10** also outperformed teriflunomide, both showing antiproliferative effects that were 30 times more potent. The DHODH-dependence of the antiproliferative effects of compounds **4** - **6** and **8** - **10** were also tested by assaying their activity in the presence of 100 μ M uridine.³⁷ As shown in Table 1, the antiproliferative effects were reverted by the addition of exogenous uridine, which strongly indicates that the compounds act as pyrimidine biosynthesis inhibitors, and thus inhibit Jurkat cell proliferation via this mechanism. The exception to this is **8**, which is probably too weak as *h*DHODH inhibitor to produce a reverse uridine-mediated effect. In order to evaluate whether the antiproliferative effects resulted from cell death, cytotoxicity was evaluated on Jurkat T cells using the CellTox green assay and the concentration of compounds that was able to cause 30 % cell death were detected. Compound **4** had no negative effect on cell viability up to 60 μ M, while **5** and **6** were found to be cytotoxic in a concentration similar to that of brequinar. Intriguingly, no negative effect on cell viability was observed for compounds **8** - **10**, for which a diphenylether was used to introduce subsite 1 interactions, even when they were tested at a concentration of 100 μ M. This result is quite

interesting as it shows how promising drug-like profiles can be obtained using this moiety for targeting subsite 1 interactions.

In order to investigate whether the immunosuppressive activity of the compounds, their effect on the proliferation of phytohaemagglutinin-activated peripheral blood mononuclear cells (PBMCs) was evaluated and compared with that of brequinar. As shown in Table 1, the antiproliferative effect of brequinar is 10 times greater than that of teriflunomide (3.74 and 54.3 μ M, respectively), which confirms earlier research. It was observed that potent activity against *h*DHODH correlates with the potent inhibition of activated PBMC proliferation for all tested compounds. This inhibition, however, can be *reversed* by the *addition of exogenous uridine*, suggesting that the immunosuppressive activity of the compounds may be due to the inhibition of *de novo* pyrimidine nucleotide synthesis.

2.4.2 Proliferation, cytotoxicity and myeloid differentiation in Leukemia cells.

In the last phase of our study, we evaluated the effects of our *h*DHODH inhibitors on two AML cell lines (U937 and THP1). We decided to compare compound **4**, judged as the best compromise between potency and cytotoxicity, triazole **2**, the top compound from the first series, which displays very low cytotoxicity, and brequinar, which was used as a positive control. In the initial experiments, we evaluated cell viability using CFSE-based assays. As shown in Figure 7A, both compound **4** and brequinar show strong and concentration-dependent cytotoxicity, while compound **2** is only able to induce cell death at high doses.

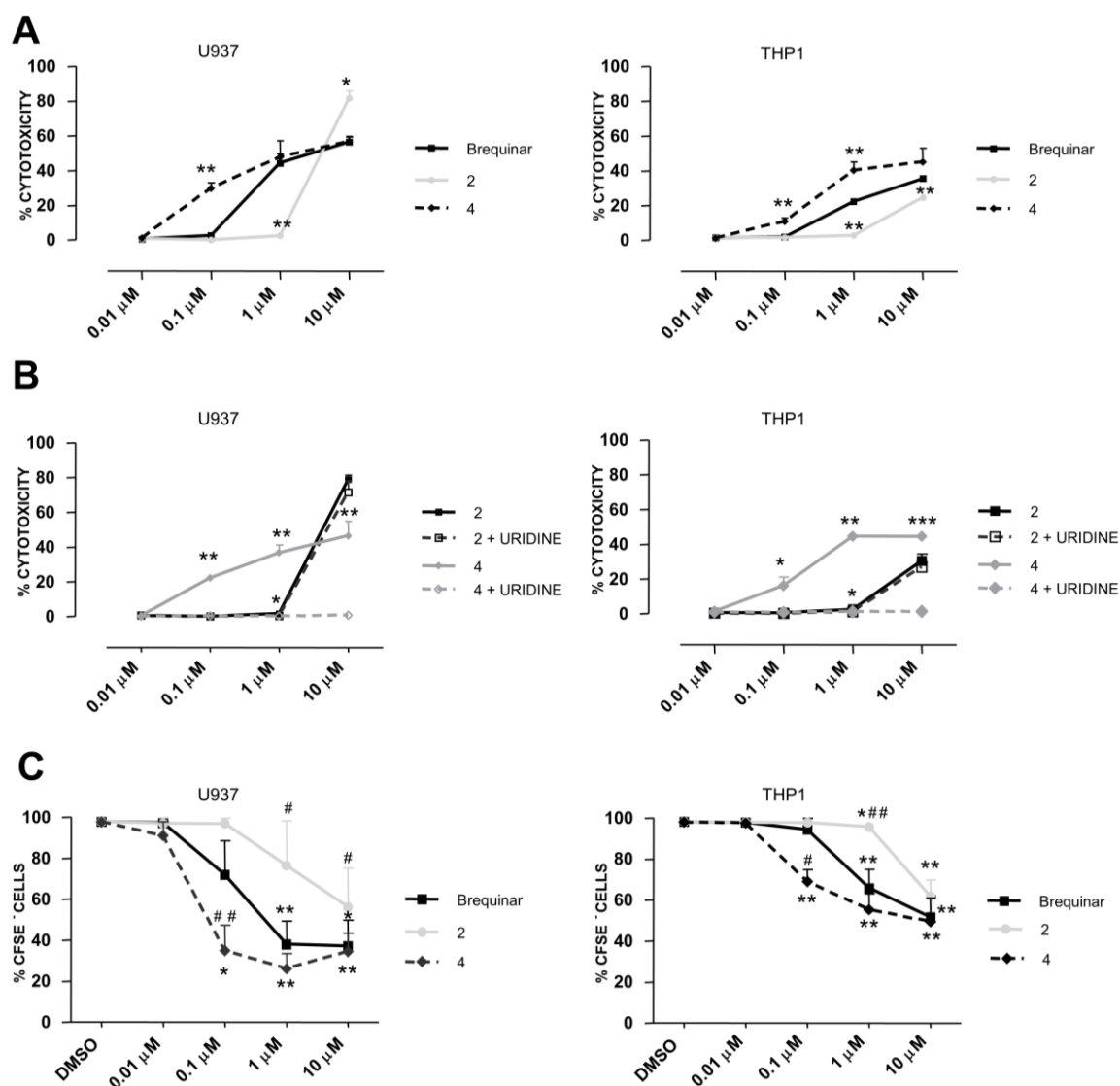


Figure 7. A) Cytotoxicity induced by different concentrations of brequinar, compound **2** and **4** on U937 and THP1. Statistical significance: * $p < 0.05$; ** $p < 0.01$ between our compounds and brequinar. B) Cytotoxicity is totally reversed when uridine is added to compound **4**, but not to compound **2**, both in U937 and THP1. Statistical significance: * $p < 0.05$; ** $p < 0.01$ between each compound \pm uridine. Uridine was added at 100 μ M concentration. C) Proliferation inhibition exerted by different concentrations of brequinar, compound **2** and **4** on U937 and THP1. Statistical significance: * $p < 0.05$; ** $p < 0.01$; *** $p < 0.001$ between treated and untreated cells (DMSO only). # $p < 0.05$ between our compounds and brequinar. DMSO = dimethyl sulfoxide, i.e., the solvent of all tested compounds.

The cytotoxicity of compound **4** was totally reversed when uridine was added, but this was not the case for compound **2** (Figure 7B). This suggests that, in the case of compound **4** cytotoxicity may only be ascribed to *h*DHODH inhibition, while cytotoxicity of compound **2** at high doses is probably associated with off-target effects. Moreover, cytotoxicity against U937 was slightly more evident than that against THP1, which probably reflects the heterogeneity of AML. CFSE-based proliferation assays were also performed and, as expected, compound **4**, brequinar and, to a lesser extent, compound **2**, all greatly reduced cell proliferation, as shown in Figure 7C. Interestingly, compound **4** seemed to be more effective than brequinar at lower concentrations both in proliferation and cytotoxicity experiments. While results from the proliferation assays were expected, cytotoxicity data, at first sight, contradicted the Jurkat-T cell experiments, which had shown our compounds' very low toxicity. However, as mature cells have a much shorter half-life than immature ones, we hypothesized that the considerable cytotoxicity observed in AML cell lines, but not in Jurkat-T cells, had to be ascribed to the differentiation induced in leukemic cells by *h*DHODH inhibitors. We therefore investigated the differentiation effect induced by compounds **2**, **4** and brequinar on our AML cell lines at several concentrations. The differentiation process was tracked by analyzing CD11b and CD14 expression, as these antigens are typically present in mature myeloid cells. In particular, cell differentiation could be best evaluated with CD11b on U937 and with CD14 on THP1; similar, but less prominent results were obtained with CD11b on THP1 (see supplementary Figure S3). Our experiments clearly demonstrated that both compound **4** and brequinar induced a strong differentiation in U937 and THP1 cells, as shown in Figure 8A, 8B and supplementary Figure S3. After the treatment with these compounds, in fact, the expression of CD11b and CD14 increased significantly day by day, depending on compound concentrations.

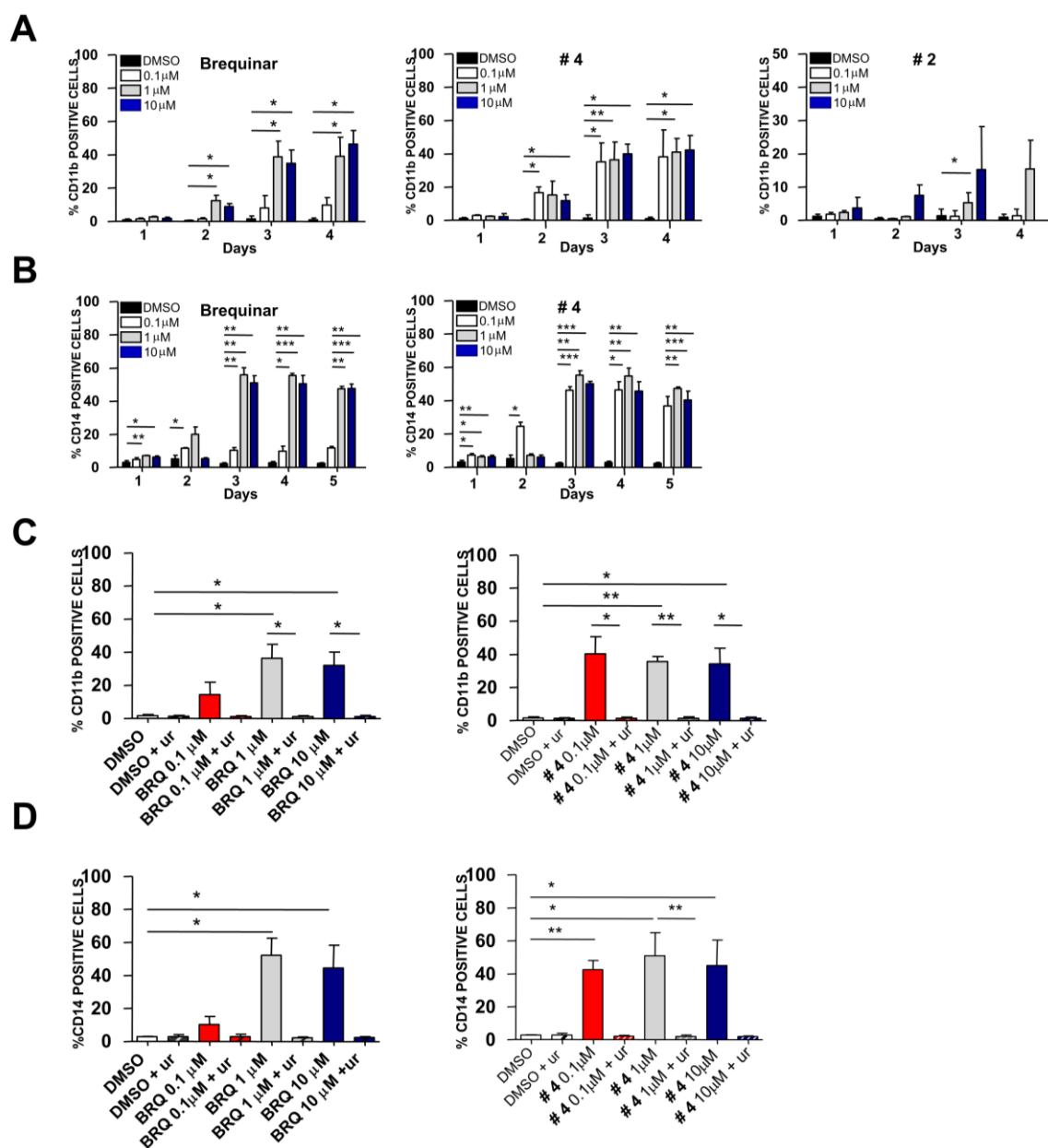


Figure 8. A) Kinetic of differentiation induced by various concentrations of brequinar, compound **4** and **2**, on U937, expressed as the proportion of CD11b positive cells. B) Kinetic of differentiation induced by various concentrations of brequinar and compound **4** on THP1, expressed as the proportion of CD14 positive cells. C) The differentiation induced on U937 by brequinar (left panel) and compound **4** (right panel) is reversed when uridine is added. The differentiation analysis is performed at day 3. D) The differentiation induced on THP1 by brequinar (left panel) and compound **4** (right panel) is reversed when uridine is added. The differentiation analysis is performed at day 3. DMSO indicates cells treated with dimethyl sulfoxide only. **#4** = compound **4**; **#2** = compound **2**; BRQ = brequinar; ur = uridine. Uridine

was added at 100 μ M concentration in all experiments. Statistical significance: * $p < 0.05$; ** $p < 0.01$; *** $p < 0.001$.

Notably, compound **4** induced a differentiation effect that was comparable to that of brequinar at a 1-log inferior concentration. Compound **2**, on the other hand, only induced a mild CD11b increase in U937 cells that only occurred at high doses (10 μ M), where it was associated with significant cell death. These data, together with the cytotoxicity results, indicated that compound **2** was not able to induce myeloid differentiation and caused off-target toxicity at high doses. For this reason, compound **2** was excluded from further experiments with THP1 and uridine.

In order to further demonstrate the connection between differentiation and *h*DHODH inhibition, the differentiation experiments were repeated in presence of uridine, and the complete rescue of the phenomenon was observed (Figure 8C, D). Differentiation experiments had to be stopped after 4 days as differentiated cells progressively died. With this in mind, we can see how compound **4** and brequinar alone caused the death of the vast majority of leukemic cells *in vitro*, even though the proportion of daily differentiating cells reached a 40 % maximum (Figure 9 and Figure S4 in supplementary). Again, compound **4** was able to induce a massive death of leukemic cells already at 0.1 μ M, i.e., at a 1-log inferior concentration compared to brequinar.

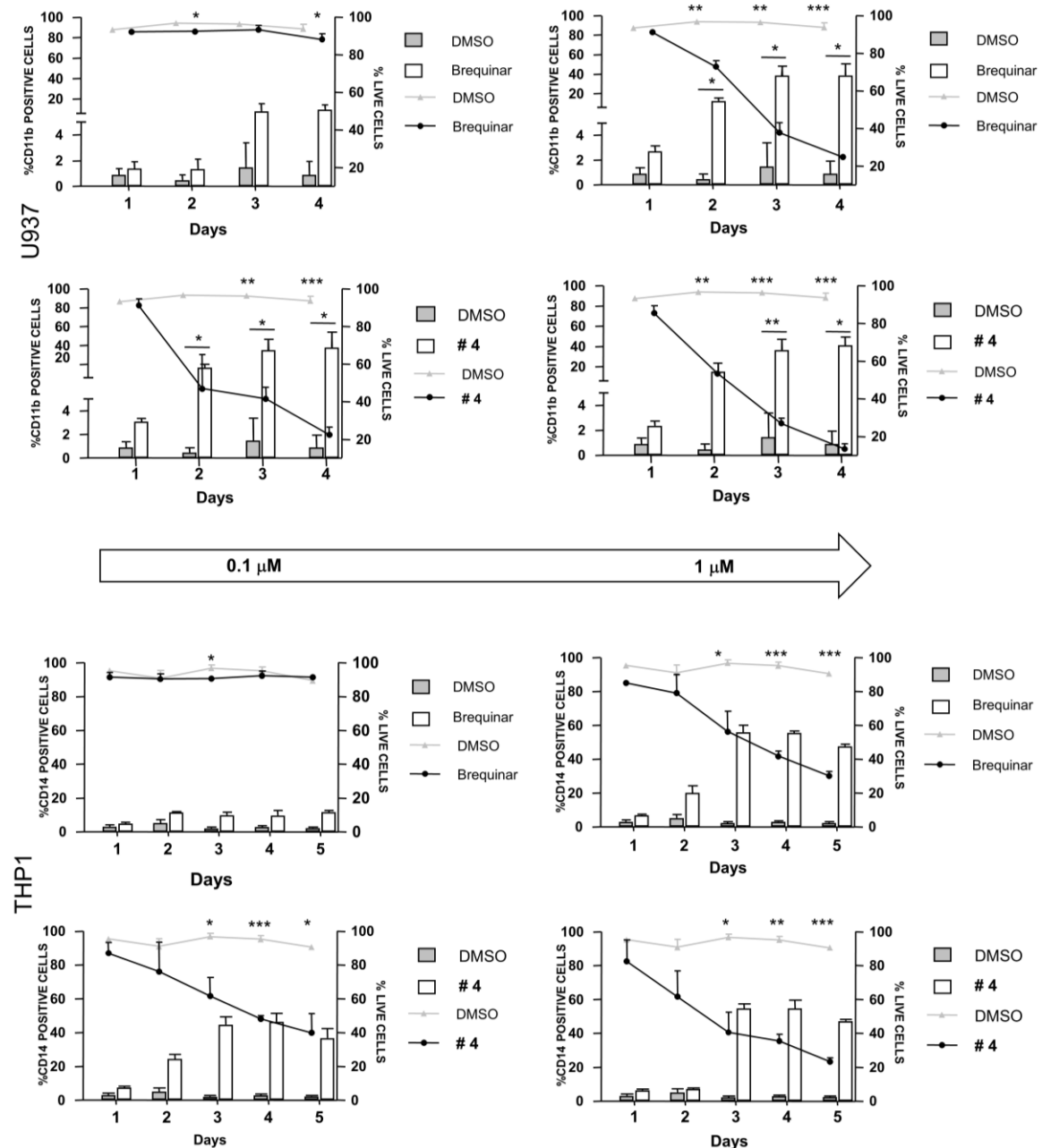


Figure 9. Parallelism between the daily proportion of differentiating cells and cells viability. The proportion of differentiating cells is expressed with bars, and the reference axis is on the left; cells viability is expressed with lines, and the reference axis is on the right. The bottom arrow indicates the concentration of drugs. Experiments were performed both on U937 and THP1 and differentiation was evaluated, respectively, with CD11b and CD14 expression. See supplementary Figure S4 for experiments with 10 μ M concentrations. Statistical significance: * $p < 0.05$; ** $p < 0.01$; *** $p < 0.001$ between treated and untreated cells. DMSO = dimethyl sulfoxide.

2.5 Physicochemical characterization and drug-like properties.

The determination of the main physicochemical properties that define the drug-like proprieties was carried out for all compounds by measuring their lipophilicity ($\log D^{7.4}$) and solubility at physiological pH. Data are reported in Table 4. Compound solubility was evaluated at pH 7.4 in phosphate buffered saline (PBS), at 37 °C to simulate body fluid, and in PBS with 2 % v/v of DMSO to explore solubility limits under *in vitro* experimental conditions. Unfortunately, all compounds showed around ten times lower solubility than brequinar. However, the values were sufficient to permit the *in vitro* tests to be performed. All compounds display good lipophilic-hydrophilic balance, with $\log D$ values that are optimal for favorable pharmacokinetic behavior; the differences between calculated $\log P$ (clogP), and measured $\log D^{7.4}$ were in agreement with the presence of significant compound ionization at physiological pH. The serum behavior of compounds **2** and **4**, selected for differentiation studies on leukemic cells, was characterized by measuring human serum stability and serum protein binding. Compounds **2** and **4** showed serum profiling that was very similar to that of reference compound brequinar; good stability and a very high percentage of protein binding (Table 5).^{38, 39}

Compound	Solubility (μM)	Solubility (μM)	clogP ^a	log D ^{7.4} ± SD ^b
	in PBS	in PBS with 2% DMSO		
Brequinar	229	449	6.39	1.83 ±0.02
Teriflunomide	2692	n.d.	n.d.	n.d.
2	956	2169	2.59	0.98 ±0.03
4	12	27	4.06	2.35 ±0.02
5	1.4	3.0	4.56	2.70 ±0.02
6	2.8	0.4	4.56	2.47 ±0.09
8	47	90	4.92	2.30 ±0.02
9	7.0	23	5.42	2.75 ±0.01
10	2.5	27	5.27	2.93 ±0.09

Table 4. ^{a)} clogP calculated using Bio-Loom for Windows, vers.1.5; ^{b)} measured using the shake flask-method. The “n.d.” notation indicates that the compound was not tested in that specific assay.

Compound	% compound	
	after 24 h in human serum	% bound
Brequinar	98	98.83
2	86	99.51
4	100	99.10

Table 5. Human serum stability and protein binding of compounds **2** and **4**, as compared to brequinar.

3. CONCLUSIONS

In this work, we have identified a novel class of inhibitors that are based on hydroxyl-pyrazolo[1,5-*a*]pyridine, an unusual bioisostere of the carboxylic acid function. Compound **4**, one of the most powerful *h*DHODH inhibitors yet discovered, has clearly been demonstrated to induce myeloid differentiation in two AML cell lines, leading to the massive death of leukemic cells. Notably, this effect was obtained at a concentration that was 1-log lower than that of the *lead* brequinar, and was restricted to leukemic cells alone. In fact, we have proven that cytotoxicity was not related to *h*DHODH inhibition *per se*, as the compound showed little or no toxicity towards Jurkat-T cells, but rather to the differentiation effect exclusively induced in AML cells via *h*DHODH inhibition. We can conclude that compound **4** displays an optimal toxicity profile and highly selective on-target activity, making it an ideal candidate for further *in vivo* studies in AML models.

4. EXPERIMENTAL

4.1. Chemistry.

4.1.1 General methods.

All chemical reagents were obtained from commercial sources (Sigma Aldrich, Alfa Aesar, FluoroChem), and used without further purification. Thin-layer chromatography (TLC), was carried out to monitor reaction progress. Analytical grade solvents (acetonitrile, diisopropyl ether, diethyl ether, dichloromethane [DCM], dimethylformamide [DMF], ethanol 99.8 % v/v, ethyl acetate [EtOAc], hexane, methanol [MeOH], petroleum ether b.p. 40 - 60°C [*petroleum ether*], toluene), were used without further purification. When needed, solvents were dried over 4 Å molecular sieves. Tetrahydrofuran (THF) was distilled from Na and benzophenone under N₂ immediately prior to use. Thin layer chromatography (TLC), on silica gel was carried out on 5 x 20 cm plates at 0.25 mm layer thickness. Anhydrous MgSO₄

was used as a drying agent for the organic phases. Compound purification was either achieved using flash column chromatography on silica gel (Merck Kieselgel 60, 230-400 mesh ASTM), and the eluents indicated in the procedures for each compound, or using CombiFlash Rf 200 (Teledyne Isco), with 5–200 mL/min, 200 psi (with automatic injection valve), and RediSep Rf Silica columns (Teledyne Isco), with the eluents indicated in the procedures for each compound. Compounds synthesized in our laboratory generally varied between 90 % and 99 % purity. Biological experiments were performed on compounds with a purity of at least 95 %. Purity was checked using two analytical methods. HPLC analyses were performed on an UHPLC chromatographic system (Perkin Elmer, Flexar). The analytical column was an UHPLC Acquity CSH Fluoro-Phenyl (2.1x100 mm, 1.7 μ m particle size, Waters). Compounds were dissolved in acetonitrile and injected through a 20 μ l loop. The mobile phase consisted of acetonitrile / water with 0.1 % trifluoroacetic acid (ratio between 60 / 40 and 40 / 60, depending on the compound's retention factor). UHPLC retention times were obtained at flow rates of 0.5 mL/min, and the column effluent was monitored at 215 and 254 nm, referenced against a 360 nm wavelength. Solubility assays, in PBS at pH 7.4, and stability assays in cell test conditions were performed on a HPLC-UV system (MERK-HITACHI), equipped with an auto sampler of 60 μ L injection volume (MERK-HITACHI AS-2000A), a binary HPLC pump (MERK-HITACHI L-6200 IP), and a diode array detector (MERK-HITACHI L-4250). LC analyses were performed using an Agilent Zorbax SB-Phenyl Column (4.6x250, 5 μ m). Melting points (m.p.), were measured on a capillary apparatus (Büchi 540). Final m.p. determination was achieved by placing the sample at a temperature 10° C below the m.p. and applying a heating rate of 1° C min⁻¹. All compounds were routinely checked by ¹H- and ¹³C-NMR and mass spectrometry. The IR spectra of solid compounds were recorded on FT-IR (PerkinElmer SPECTRUM BXII, KBr dispersions), using the diffuse reflectance apparatus DRIFT ACCY. MS spectra were either performed on a Finnigan-Mat TSQ-700 (70 eV, direct inlet for chemical ionization [CI]), or a

Waters Micromass ZQ equipped with an ESCi source for electrospray ionization mass spectra. ^1H - and ^{13}C -NMR spectra were either performed on a Bruker Avance 300 instrument or a JEOL ECZR600. The following abbreviations are used for coupling patterns: br = broad, s = singlet, d = doublet, dd = doublet of doublets, t = triplet, q = quartet, m = multiplet. Chemical shifts (δ) are given in parts per million (ppm). In this work protons and carbons are labelled (*a*, *b*, *c*, *d*, *e*, *f*, *g*, *h*, *l*, *m*, *n* and *o*) according to Scheme 2. Values marked with an asterisk are interchangeable. Detailed ^{13}C spectra of tetrafluorinated biphenyl compounds (final compounds **4** – **7** and intermediates **22a** - **c**), have not been entirely reported due to their especially complicated patterns (attributable to the multiple couplings between fluorine and carbon atoms). For these spectra, only the ^{13}C signals caused by the heterocyclic substructure and non-aromatic carbons are assigned. For the intermediates **15a**, **15b**, **15c**, **16a**, **17a**, **18a**, **19a**, **20a** and final compounds **4** – **6** and **8** – **10**, HRMS spectra were recorded on an LTQ Orbitrap mass spectrometer (Thermo Scientific, Bremen, Germany), equipped with an atmospheric pressure interface and an ESI ion source instrument. Compounds **24**⁴⁰ and **25**⁴⁰ were prepared according to previously-described procedures.

The designed compounds have been examined for known classes of assay interference compounds (Pan Assay Interference Compounds) excluding any interference.

General procedures for the synthesis of 15a, 15b, 15c. A solution of hydroxylamine-O-sulfonic acid (HOSA, 18 g, 0.16 mol) and the appropriate type **11** pyridine (3 eq) was stirred in water (150 mL) at 90 °C for 1 h. The solution was cooled to room temperature and K_2CO_3 (21.99 g, 0.16 mol) was then added. The resulting suspension was concentrated under vacuum and the residue taken up with abs EtOH (200 mL). The resulting suspension was filtered and diethyl malonate (50.98 g, 48.56 mL, 0.32 mol) was added to the filtrate. The solution was stirred at 90 °C for 3 h and then concentrated under vacuum. The residue was purified via flash chromatography (eluent: dichloromethane / EtOH 9/1 v/v), to afford a brownish sticky oil (type **14**), this latter was used in the subsequent step without any further

purification. Potassium tert-butoxide (17.86 g, 1 eq) was added portionwise to a solution of type **14** in dry THF (300 mL). The resulting dark-orange suspension was stirred at room temperature for some minutes until complete conversion was observed, after which it was concentrated under vacuum. The residue was diluted and acidified to pH 2 using 0.5 N HCl (250 mL), and extracted with ethyl acetate (2 x 150 mL). The organic phases were collected, dried and evaporated under vacuum to afford a yellowish crude oil that was purified by flash chromatography (eluent: dichloromethane / MeOH 9/1 v/v), to afford the desired compounds as white solids.

Ethyl 2-hydroxypyrazolo[1,5-a]pyridine-3-carboxylate (15a). Pale orange solid (m.p. 150.0 - 151.3 °C, from methanol). Yield 21 %. ¹H-NMR (300 MHz, DMSO): δ 1.29 (*t*, 3H, *J* = 7.0 Hz, -CH₂CH₃), 4.24 (*q*, 2H, *J* = 7.0 Hz, -CH₂CH₃), 6.98 (*t*, 1H, *J* = 6.7 Hz, *H-b*), 7.48 (*t*, 1H, *J* = 7.5 Hz, *H-c*), 7.84 (*d*, 1H, *J* = 8.8 Hz, *H-d*), 8.55 (*d*, 1H, *J* = 6.7 Hz, *H-a*), 11.14 (*s*, 1H, -OH); ¹³C-NMR (75 MHz, DMSO): δ 14.5 (-CH₂CH₃), 58.9 (-OCH₂CH₃), 86.4 (*C-f*), 113.1 (*C-b*), 116.9 (*C-d*), 128.2 (*C-c*), 129.2 (*C-a*), 141.5 (*C-e*), 162.7 (*C-h*)*, 164.5 (*C-g*)*; MS (CI) 207 (*M*+1). IR (KBr) ν (cm⁻¹): 3094, 2979, 1700, 1639, 1559, 1534, 1448, 1330, 1246, 1212, 1156, 1107, 1026. ESI-HRMS (*m/z*) [*M* + *H*]⁺ calcd. for C₁₀H₁₁N₂O₃ 207.0764, obsd. 207.0769.

Ethyl 2-hydroxy-7-methyl-pyrazolo[1,5-a]pyridine-3-carboxylate (15b). White solid (m.p. 113.8 - 114.6 °C; from trituration with diisopropyl ether). Yield 19 %. ¹H-NMR (300 MHz, DMSO): δ 1.30 (*t*, 3H, *J* = 7.0 Hz, -OCH₂CH₃), 2.60 (*s*, 3H, Ar-CH₃), 4.24 (*q*, 2H, *J* = 7.0 Hz, -OCH₂CH₃), 6.91 (*d*, 1H, *J* = 6.9 Hz, *H-b*), 7.42 (*t*, 1H, *J* = 7.9 Hz, *H-c*), 7.75 (*d*, 1H, *J* = 8.7 Hz, *H-d*), 11.20 (*s*, 1H, -OH); ¹³C-NMR (75 MHz, DMSO): δ 14.5 (-OCH₂CH₃), 17.4 (Ar-CH₃), 58.9 (-OCH₂CH₃), 86.5 (*C-f*), 112.67 (*C-b*), 114.5 (*C-d*), 128.1 (*C-c*), 138.3 (*C-a*), 141.8 (*C-e*), 162.8 (*C-h*)*, 164.2 (*C-g*)*; MS (CI) 221 (*M*+1). IR (KBr) ν (cm⁻¹): 3069, 2991, 1700, 1637, 1560, 1533, 1385, 1330, 1219, 1163, 1104, 1068, 1039. ESI-HRMS (*m/z*) [*M* + *H*]⁺ calcd. for C₁₁H₁₃N₂O₃ 221.0921, obsd. 221.0926.

Ethyl 2-hydroxy-5-methyl-pyrazolo[1,5-a]pyridine-3-carboxylate (15c). White solid (m.p. 123.4 - 126.6 °C; from trituration with diisopropyl ether). Yield 19 %. ¹H-NMR (300 MHz, DMSO): δ 1.29 (*t*, 3H, *J* = 7.1 Hz, -OCH₂CH₃), 2.37 (*s*, 3H, Ar-CH₃), 4.23 (*q*, 2H, *J* = 7.1 Hz, -OCH₂CH₃), 6.82 (*dd*, 1H, *J* = 6.9, 1.7 Hz, *H-b*), 7.61 (*s*, 1H, *H-d*), 8.42 (*d*, 1H, *J* = 6.9 Hz, *H-a*), 11.04 (*br s*, 1H, -OH); ¹³C-NMR (75 MHz, DMSO): δ 14.5 (-OCH₂CH₃), 21.0 (Ar-CH₃), 58.9 (-OCH₂CH₃), 85.6 (*C-f*), 115.2 (*C-b*)^{*}, 115.6 (*C-d*)^{*}, 128.5 (*C-a*), 139.1(*C-c*), 141.5 (*C-e*), 162.8 (*C-h*)^{*}, 164.6 (*C-g*)^{*}; MS (CI) 221 (*M*+1). IR (KBr) ν (cm⁻¹): 3064, 2986, 1654, 1561, 1498, 1435, 1305, 1250, 1211, 1185, 1112, 1029. ESI-HRMS (*m/z*) [*M* + *H*]⁺ calcd. for C₁₁H₁₃N₂O₃ 221.0921, obsd. 221.0926.

Ethyl 2-methoxypyrazolo[1,5-a]pyridine-3-carboxylate (16a) and ethyl 1-methyl-2-oxo-1,2-dihydropyrazolo[1,5-a]pyridine-3-carboxylate (17a) from **15a**. Cesium carbonate (1.48 g, 10.67 mmol) was added to a solution of **15a** (1.00 g, 4.85 mmol) in dry THF (30 mL), while stirred under nitrogen. Methyl iodide (2.07 g, 7.28 mmol) was then added to the resulting dark orange suspension and the mixture was stirred at 40 °C overnight. The suspension was then concentrated under vacuum, taken up with water (100 mL) and extracted with EtOAc (3 x 100 mL). The organic layers were collected, dried and evaporated under vacuum to afford a crude material that was purified by flash chromatography, (eluent: petroleum ether / EtOAc 8/2 v/v and then eluent: dichloromethane / MeOH 9:1 v/v). The structures were determined unequivocally using heteronuclear 2D-NMR (HSQC, HMBC and NOESY, see supplementary information).

16a). White solid (m.p: 128.9 - 129.4 °C, from trituration with diisopropyl ether). Yield 59 %. ¹H-NMR (300 MHz DMSO): δ 1.29 (*t*, 3H, *J* = 7.1 Hz, -OCH₂CH₃), 4.00 (*s*, 3H, -OCH₃) 4.23 (*q*, 2H, *J* = 7.1 Hz, -OCH₂CH₃), 7.02 (*td*, 1H, *J* = 6.9 Hz, 1.0 Hz, *H-b*), 7.52 (*t*, 1H, *J* = 7.9 Hz, *H-c*), 7.88 (*d*, 1H, *J* = 8.9 Hz, *H-d*), 8.65 (*d*, 1H, *J* = 6.8 Hz, *H-a*); ¹³C-NMR (75 MHz DMSO): δ 14.5(-OCH₂CH₃), 56.5 (-OCH₃), 59.0 (-OCH₂CH₃), 86.7 (*C-f*), 113.2 (*C-b*), 117.2 (*C-d*), 128.8 (*C-c*), 129.6 (*C-a*), 142.1 (*C-e*), 162.0 (*C-h*)^{*}, 165.0 (*C-g*)^{*}; MS (CI) 221(*M*+1).

IR (KBr) ν (cm⁻¹): 3085, 3042, 2990, 1691, 1517, 1449, 1407, 1300, 1245, 1157, 1105, 1023; ESI-HRMS (m/z) [M + H]⁺ calcd. for C₁₁H₁₃N₂O₃ 221.0921, obsd. 221.0924.

17a). Orange solid (m.p. 217.8 - 224.2 °C dec., from trituration with diisopropyl ether). Yield 35 %. ¹H-NMR (300 MHz DMSO): δ 1.28 (t, 3H, J = 7.0 Hz, -OCH₂CH₃), 3.58 (s, 3H, -NCH₃), 4.21 (q, 2H, J = 7.0 Hz -OCH₂CH₃), 7.10 (t, 1H, J = 6.6 Hz, *H-b*), 7.66 (t, 1H, J = 7.8 Hz, *H-c*), 7.90 (d, 1H, J = 8.6 Hz, *H-d*), 8.57 (d, 1H, J = 6.3 Hz, *H-a*); ¹³C-NMR (75 MHz DMSO): δ 14.5 (-CH₂CH₃), 28.9 (-NCH₃), 59.3 (-CH₂CH₃), 84.2 (C-f), 113.3 (C-b), 116.7 (C-d), 125.8 (C-a), 132.9 (C-c), 142.6 (C-e), 160.6 (C-g), 164.1 (C-h); MS(CI) 221(M+1). IR (KBr) ν (cm⁻¹): 3507, 3069, 3025, 2977, 1687, 1625, 1511, 1477, 1437, 1256, 1227, 1189, 1093, 1024; ESI-HRMS (m/z) [M + H]⁺ calcd. for C₁₁H₁₃N₂O₃ 221.0921, obsd. 221.0925.

Ethyl N-benzyl-2-oxo-pyrazolo[1,5-a]pyridine-3-carboxylate (18a) and ethyl 2-benzyloxypyrazolo[1,5-a]pyridine-3-carboxylate (19a) from **15a**. Benzyl bromide (3.0 g, 14.50 mmol) was added dropwise to a mixture of **15a** (2.74 g, 16.00 mmol) and cesium carbonate (11.85 g, 36.40 mmol) in dry DMF (50 mL). The reaction mixture was stirred for 18 hours at room temperature and water (100 mL) was then added. The mixture was extracted with EtOAc (3 x 100 mL), the combined organic layer was washed with brine, and then dried and evaporated under reduced pressure to get a colorless oil. This latter provided two spots on TLC (eluent: petroleum ether / EtOAc 80/20 v/v), which were ascribed to the two pyrazolo[1,5-a]-pyridine isomers. The mixture was separated using flash chromatography (eluent: *petroleum ether* / EtOAc 80/20 v/v, then eluent: dichloromethane / MeOH 9:1 v/v). The structures were determined unequivocally using heteronuclear 2D-NMR (HSQC, HMBC and NOESY, see supplementary information).

18a) Second isomer eluted, white solid (m.p: 172.3 - 174.0 °C, from EtOAc / diisopropyl ether 1/1 v/v). Yield 21 %. ¹H-NMR (300 MHz DMSO): δ 1.28 (t, 3H, J = 7.1 Hz -OCH₂CH₃), 4.22 (q, 2H, J = 7.1 Hz -OCH₂CH₃), 5.43 (s, 2H, -NCH₂Ph), 6.95 (td, 1H, J = 7.1, 1.0 Hz, *H-b*), 7.18 - 7.38 (m, 5H, *H-m*, *H-o*, *H-n*), 7.59 (t, 1H, J = 8.0 Hz, *H-c*), 7.92 (d,

1H, J = 8.8 Hz, *H-d*), 8.41 (*d*, 1H, J = 6.9 Hz, *H-a*); ¹³C-NMR (75 MHz DMSO): δ 14.4 (-OCH₂CH₃), 44.5 (-NCH₂Ph), 59.4 (-OCH₂CH₃), 84.3 (*C-f*), 113.3 (*C-b*), 117.2 (*C-d*), 126.0 (*C-a*), 128.0 (*C-m*), 128.8 (*C-o*), 129.8 (*C-n*), 133.3 (*C-c*), 134.8 (*C-l*), 143.6 (*C-e*), 160.8 (*C-g*)*, 164.0 (*C-h*)*; MS (CI) 297 (M+1). IR (KBr) ν (cm⁻¹): 3084, 3056, 2977, 1699, 1631, 1547, 1511, 1464, 1431, 1345, 1238, 1135, 1030. ESI-HRMS (m/z) [M + H]⁺ calcd. for C₁₇H₁₆N₂O₃ 297.1234, obsd. 297.1239.

19a) First isomer eluted, pale yellow solid (m.p: 100.0 - 100.8 °C, from trituration with diisopropyl ether). Yield 75 %. ¹H-NMR (300 MHz DMSO): δ 1.30 (*t*, 3H, J = 7.1 Hz -OCH₂CH₃), 4.24 (*q*, 2H, J = 7.1 Hz -OCH₂CH₃), 5.44 (*s*, 2H, -OCH₂Ph), 7.04 (*t*, 1H, J = 6.9 Hz, *H-b*), 7.29 – 7.45 (*m*, 3H, *H-o*, *H-n*), 7.47 - 7.59 (*m*, 3H, *H-m*, *H-c*), 7.91 (*d*, 1H, J = 8.8 Hz, *H-d*), 8.67 (*d*, 1H, J = 6.8 Hz, *H-a*); ¹³C-NMR (75 MHz DMSO): δ 14.4 (-OCH₂CH₃), 59.0 (-OCH₂CH₃), 70.2 (-OCH₂Ph), 87.0 (*C-f*), 113.3 (*C-b*), 117.2 (*C-d*), 127.4 (*C-m*), 127.9 (*C-o*), 128.3 (*C-n*), 128.9 (*C-c*), 129.6 (*C-a*), 136.6 (*C-l*), 142.0 (*C-e*), 161.9 (*C-h*)*, 164.3 (*C-g*)*; MS (CI) 297 (M+1). IR (KBr) ν (cm⁻¹): 3097, 3033, 2978, 1675, 1635, 1530, 1515, 1440, 1364, 1251, 1208, 1141, 1053, 1021. ESI-HRMS (m/z) [M + H]⁺ calcd. for C₁₇H₁₆N₂O₃ 297.1234, obsd. 297.1240.

Ethyl N-benzyl-7-methyl-2-oxo-pyrazolo[1,5-a]pyridine-3-carboxylate (18b) and ethyl 2-benzyloxy-7-methyl-pyrazolo[1,5-a]pyridine-3-carboxylate (19b) from **15b**. Benzyl bromide (0.85 g, 4.99 mmol) was added dropwise to a mixture of **15b** (1.00 g, 4.54 mmol) and cesium carbonate (3.70 g, 11.35 mmol) in dry DMF (25 mL). The reaction mixture was stirred for 5 hours at room temperature before adding water (100 mL). The mixture was extracted using EtOAc (3 x 100 mL) the combined organic layer was washed with brine, dried and evaporated under reduced pressure to afford a colorless oil. This latter showed two spots on TLC (eluent: petroleum ether / EtOAc 80/20 v/v), ascribed to the two pyrazolo[1,5-a]-pyridine isomers. The mixture was separated using flash chromatography (eluent: petroleum ether / EtOAc 90/10 v/v, then eluent: dichloromethane / MeOH 9:1 v/v).

18b) Second isomer eluted, white solid (m.p. 145.0 - 147.8 °C; from trituration with diisopropyl ether). Yield 5 %. ¹H-NMR (600 MHz DMSO): δ 1.29 (*t*, 3H, *J* = 7.1 Hz - OCH₂CH₃), 2.62 (*s*, 3H, Ar-CH₃), 4.22 (*q*, 2H, *J* = 7.1 Hz, -OCH₂CH₃), 5.41 (*s*, 2H, -NCH₂Ph), 6.75 (*d*, 1H, *J* = 7.1 Hz, *H-b*), 6.96 (*d*, 2H, *J* = 7.5 Hz, *H-m*), 7.22 (*t*, 1H, *J* = 7.2 Hz, *H-o*), 7.27 (*t*, 2H, *J* = 7.4 Hz, *H-n*), 7.53 (*t*, 1H, *J* = 8.0 Hz, *H-c*), 7.86 (*d*, 1H, *J* = 8.7 Hz, *H-d*); ¹³C-NMR (151 MHz DMSO): δ 14.6 (-OCH₂CH₃), 20.0 (Ar-CH₃), 50.4 (-NCH₂Ph), 58.6 (-OCH₂CH₃), 83.8 (*C-f*), 114.2 (*C-b*)*, 114.8 (*C-d*)*, 126.2 (*C-m*), 127.8 (*C-o*), 128.9 (*C-n*), 134.3 (*C-c*), 135.5 (*C-l*), 140.3 (*C-a*), 148.5 (*C-e*), 163.1 (*C-g*)*, 165.0 (*C-h*)*; MS (ESI) 311 (M+1). IR (KBr) ν (cm⁻¹): 2975, 1718, 1647, 1559, 1516, 1437, 1318, 1250, 1154, 1129, 1071.

19b) First isomer eluted, pale yellow solid (m.p. 74.3 - 75.9 °C; from trituration with diisopropyl ether). Yield 93 %. ¹H-NMR (600 MHz CDCl₃): δ 1.41 (*t*, 3H, *J* = 7.1 Hz - OCH₂CH₃), 2.68 (*s*, 3H, Ar-CH₃), 4.37 (*q*, 2H, *J* = 7.1 Hz -OCH₂CH₃), 5.54 (*s*, 2H, -OCH₂Ph), 6.68 (*d*, 1H, *J* = 7.0 Hz, *H-b*), 7.24 – 7.32 (*m*, 2H, *H-o*, *H-c*), 7.37 (*t*, 2H, *J* = 7.6 Hz, *H-n*), 7.58 (*d*, 2H, *J* = 7.4 Hz, *H-m*), 7.89 (*d*, 1H, *J* = 8.8 Hz, *H-d*); ¹³C-NMR (151 MHz CDCl₃): δ 14.7 (-OCH₂CH₃), 17.9 (Ar-CH₃), 59.7 (-OCH₂CH₃), 70.8 (-OCH₂Ph), 88.4 (*C-f*), 112.2 (*C-b*), 115.7 (*C-d*), 127.7 (*C-m*), 127.8 (*C-o*), 127.9 (*C-c*), 128.4 (*C-n*), 137.2 (*C-l*), 138.9 (*C-a*), 143.2 (*C-e*), 163.6 (*C-h*)*, 164.7 (*C-g*)*; MS (ESI) 311 (M+1). IR (KBr) ν (cm⁻¹): 3061, 3026, 2974, 1684, 1640, 1539, 1516, 1448, 1358, 1274, 1214, 1135, 1107, 1011.

Ethyl N-benzyl-5-methyl-2-oxo-pyrazolo[1,5-a]pyridine-3-carboxylate (18c) and ethyl 2-benzyloxy-5-methyl-pyrazolo[1,5-a]pyridine-3-carboxylate (19c) from **15c**. Benzyl bromide (0.85 g, 4.99 mmol), was added dropwise to a mixture of **15c** (1.00 g, 4.54 mmol) and cesium carbonate (3.70 g, 11.35 mmol) in dry DMF (25 mL). The reaction mixture was stirred for 4 hours at room temperature and water (100 mL), was then added. The mixture was extracted using EtOAc (4 x 100 mL), the combined organic layer was washed with brine, dried and evaporated under reduced pressure to get a colorless oil. This latter showed two

spots on TLC (eluent: petroleum ether / EtOAc 80/20 v/v), ascribed to the two pyrazolo[1,5-a]-pyridine isomers. The mixture was separated using flash chromatography (eluent: petroleum ether / EtOAc 90/10 v/v, then eluent: dichloromethane / MeOH 9:1 v/v).

18c) Second isomer eluted, white solid (m.p. 167.1 – 169.5 °C; from trituration with diisopropyl ether). Yield 29 %. ¹H-NMR (600 MHz DMSO): δ 1.45 (t, 3H, J = 7.1 Hz -OCH₂CH₃), 3.53 (s, 3H, Ar-CH₃), 4.38 (q, 2H, J = 7.1 Hz, -OCH₂CH₃), 5.56 (s, 2H, -NCH₂Ph), 6.97 (dd, 1H, J = 7.0 Hz, 1.8 Hz, *H-b*), 7.37 (d, 2H, J = 7.3 Hz, *H-m*), 7.43 (t, 1H, J = 7.3 Hz, *H-o*), 7.49 (t, 2H, J = 7.4 Hz, *H-n*), 7.90 (s, 1H, *H-d*), 8.48 (d, 1H, J = 7.0 Hz, *H-a*); ¹³C-NMR (151 MHz DMSO): δ 14.6 (-OCH₂CH₃), 21.1 (Ar-CH₃), 43.7 (-NCH₂Ph), 58.4 (-OCH₂CH₃), 82.8 (*C-f*), 114.4 (*C-b*), 115.2 (*C-d*), 124.6 (*C-a*), 127.2 (*C-m*), 128.0 (*C-o*), 128.9 (*C-n*), 134.1 (*C-l*), 142.8 (*C-c*), 144.0 (*C-e*), 160.4 (*C-g*)*, 163.3 (*C-h*)*; MS (ESI) 311 (M+1). IR (KBr) ν (cm⁻¹): 3087, 2979, 1701, 1632, 1539, 1502, 1430, 1365, 1305, 1243, 1160, 1113, 1040.

19c) First isomer eluted, pale yellow solid (m.p. 81.5 – 83.0 °C; from trituration with diisopropyl ether). Yield 58 %. ¹H-NMR (600 MHz CDCl₃): δ 1.41 (t, 3H, J = 7.1 Hz -OCH₂CH₃), 2.42 (s, 3H, Ar-CH₃), 4.37 (q, 2H, J = 7.1 Hz -OCH₂CH₃), 5.48 (s, 2H, -OCH₂Ph), 6.66 (dd, 1H, J = 6.90 Hz, 1.9 Hz, *H-b*), 7.31 (t, 1H, J = 7.4 Hz, *H-o*), 7.38 (t, 2H, J = 7.6 Hz, *H-n*), 7.55 (d, 2H, J = 7.5 Hz, *H-m*), 7.79 (s, 1H, *H-d*), 8.15 (d, 1H, J = 6.9 Hz, *H-a*); ¹³C-NMR (151 MHz, CDCl₃): δ 14.7 (-OCH₂CH₃), 21.7 (Ar-CH₃), 59.7 (-OCH₂CH₃), 70.7 (-OCH₂Ph), 87.6 (*C-f*), 115.0 (*C-b*), 117.1 (*C-d*), 127.3 (*C-m*), 127.9 (*C-o*), 128.1 (*C-a*), 128.5 (*C-n*), 136.9 (*C-l*), 139.3 (*C-c*), 143.1 (*C-e*), 163.6 (*C-h*)*, 165.2 (*C-g*)*; MS (ESI) 311 (M+1). IR (KBr) ν (cm⁻¹): 3048, 2981, 1687, 1641, 1540, 1519, 1443, 1364, 1289, 1252, 1215, 1172, 1141, 1054.

General procedure for base-catalyzed ester hydrolysis (20a - c). 5 M NaOH (5 eq.), was added to a solution of the appropriate ester in ethanol. The solution was stirred for 5 hours at 70 °C, then neutralized with 6 M HCl and concentrated under reduced pressure. 2 M HCl was

added at 0 °C until pH 2 was reached and the resulting suspension was filtered to get the corresponding acid.

2-Benzyloxypyrazolo[1,5-a]pyridine-3-carboxylic acid (20a). Obtained from **19a**. White solid (m.p. 159.9 – 160.5 °C; from trituration with diisopropyl ether). Yield 99 %. ¹H-NMR (300 MHz DMSO): δ 5.43 (*s*, 2H, -OCH₂Ph), 7.01 (*t*, 1H, *J* = 6.50 Hz *H-b*), 7.28 – 7.45 (*m*, 3H, *H-o*, *H-n*), 7.46 -7.57 (*m*, 3H, *H-m*, *H-c*), 7.93 (*d*, 1H, *J* = 8.80 Hz, *H-d*), 8.65 (*d*, 1H, *J* = 6.80 Hz, *H-a*), 12.10 (*s*, 1H, COOH); ¹³C-NMR (75 MHz, DMSO): δ 71.1 (-OCH₂Ph), 88.4 (*C-f*), 114.0 (*C-b*), 118.2 (*C-d*), 128.6 (*C-m*), 128.8 (*C-o*), 129.2 (*C-n*), 129.3 (*C-c*), 130.3 (*C-a*), 137.5 (*C-l*), 143.2 (*C-e*), 164.3 (*C-g*)*, 165.2 (*C-h*)*; MS(CI) 225 (M-CO₂+1); IR (KBr) ν (cm⁻¹): 2894, 2650, 1654, 1628, 1527, 1508, 1477, 1454, 1438, 1371, 1332, 1302, 1258, 1211, 1183, 1133, 1080, 1006; ESI-HRMS (*m/z*) [M + H]⁺ calcd. for C₁₅H₁₃N₂O₃ 269.0921, obsd. 269.0926.

2-Benzyloxy-7-methyl-pyrazolo[1,5-a]pyridine-3-carboxylic acid (20b). Obtained from **19b**. White solid (m.p. 181.1 - 181.8 °C; from trituration with diisopropyl ether). Yield 72 %. ¹H-NMR (600 MHz DMSO): δ 2.65 (*s*, 3H, Ar-CH₃), 5.46 (*s*, 2H, -OCH₂Ph), 6.94 (*d*, 1H, *J* = 7.0 Hz, *H-b*), 7.34 (*t*, 1H, *J* = 7.3 Hz, *H-c*), 7.40 (*t*, 2H, *J* = 7.5 Hz, *H-n*), 7.44 (*t*, 1H, *J* = 8.0 Hz, *H-o*), 7.55 (*d*, 2H, *J* = 7.3 Hz *H-m*), 7.83 (*d*, 1H, *J* = 8.7 Hz, *H-d*), 12.10 (*s*, 1H, -COOH); ¹³C-NMR (151 MHz, DMSO): δ 17.8 (Ar-CH₃), 70.7 (-OCH₂Ph), 88.2 (*C-f*), 113.0 (*C-b*), 115.5 (*C-d*), 128.5 (*C-o*), 128.6 (*C-m*), 128.9 (*C-n*), 128.9 (*C-c*), 137.2 (*C-l*), 139.1 (*C-a*), 143.2 (*C-e*), 164.2 (*C-g*)*, 164.4 (*C-h*)*; MS (ESI) 283 (M+1). IR (KBr) ν (cm⁻¹): 3030, 2632, 1657, 1632, 1560, 1509, 1450, 1364, 1286, 1215, 1154, 1129, 1062, 1007, 962.

2-Benzyloxy-5-methyl-pyrazolo[1,5-a]pyridine-3-carboxylic acid (20c). Obtained from **19c**. White solid (m.p. 174.3 - 174.9°C; from trituration with diisopropyl ether). Yield 96 %. ¹H-NMR (600 MHz DMSO): δ 2.39 (*s*, 3H, Ar-CH₃), 5.40 (*s*, 2H, -OCH₂Ph), 6.85 (*d*, 1H, *J* = 6.9 Hz, *H-b*), 7.34 (*t*, 1H, *J* = 7.3 Hz, *H-o*), 7.40 (*t*, 2H, *J* = 7.5 Hz, *H-n*), 7.50 (*d*, 2H, *J* = 7.4 Hz, *H-m*), 7.71 (*s*, 1H, *H-d*), 8.52 (*d*, 1H, *J* = 6.9 Hz, *H-a*), 12.01 (*s*, 1H, COOH); ¹³C-NMR

(151 MHz, DMSO): δ 21.0 (Ar-CH₃), 70.1 (–OCH₂Ph), 86.7 (C-f), 115.3 (C-b)*, 116.0 (C-d)*, 127.8 (C-m), 128.0 (C-o), 128.4 (C-n), 128.8 (C-a), 136.7 (C-l), 139.5 (C-c), 142.4 (C-e), 163.6 (C-h)*, 164.5 (C-g)*; MS (ESI) 283 (M+1). IR (KBr) ν (cm⁻¹): 2887, 2629, 1662, 1632, 1534, 1507, 1458, 1357, 1312, 1254, 1206, 1140, 1116, 1033, 997, 962.

General procedure for the synthesis of pyrazolo[1,5-a]pyridine related amides 22a - c. 2 M Oxalyl chloride in dry dichloromethane (3.0 mmol), and dry DMF (1 drop), were added to a cooled (0 °C), solution of the related pyrazolo[1,5-a]pyridine acid (1.0 mmol) **20a-c**, in dry THF (20 mL), under a nitrogen atmosphere. The obtained solution was stirred at room temperature for 2 hours. The solution was then concentrated under reduced pressure and the residue dissolved in dry THF (10 mL, this step was repeated three times). The resulting acyl chloride was immediately used without any further purification. Trimethylaluminium (2.0 M in hexane, 1.5 mmol) was added to a solution of the 2,3,5,6-tetrafluoro-4-phenylaniline **21** (1.1 mmol), in dry toluene (15 mL), under a nitrogen atmosphere. The resulting mixture was stirred for 2 hours at room temperature producing a brown suspension, which was then quantitatively portionwise transferred to a solution of a previously-described acyl chloride in dry toluene (30 mL). The mixture was heated overnight at 90 °C and then cooled to r.t. The reaction was quenched with 1 M HCl. The layers were resolved and the aqueous phase was exhaustively extracted using EtOAc. The combined organic layer was washed with 1 M NaOH and brine, dried and the solvent was evaporated under reduced pressure. The crude product was purified by column chromatography.

1-Benzyl-2-oxo-N-(2,3,5,6-tetrafluoro-[1,1'-biphenyl]-4-yl)-1,2-dihydropyrazolo[1,5-a]pyridine-3-carboxamide (22a). Obtained from **20a**, flash chromatography (eluent: *petroleum ether* / EtOAc 90:10 v/v). Pale yellow solid (m.p. 223.8 - 225.9 °C; from trituration with diisopropyl ether). Yield 45 %. ¹H NMR (300 MHz, CDCl₃): δ 5.48 (*s* 2H, -NCH₂Ph), 6.76 (*t*, 1H, *J* = 7.0 Hz, *H-b*), 7.19 – 7.58 (*m*, 11H, *aromatic protons* and *H-c*), 7.73 (*d*, 1H, *J* = 7.0 Hz, *H-d*), 8.28 (*d*, 1H, *J* = 8.8 Hz, *H-a*), 9.98 (*s*, 1H, -NH); ¹³C NMR (75

MHz, CDCl₃): δ 45.6 (-NCH₂Ph), 87.1 (*C-f*), 112.9 (*C-b*), 118.3 (*C-d*), 123.0 (*C-a*), 127.1, 128.7, 128.9, 129.1, 129.6, 130.3, 131.8, 132.5, 142.5, 161.7 (*C-g*)*, 162.1 (*C-h*)*; MS (ESI) 492 (M+1). IR (KBr) ν (cm⁻¹): 3227, 3101, 3063, 1667, 1628, 1519, 1484, 1438, 1313, 1239, 1172, 1152, 1113, 1076, 1004, 972.

1-Benzyl-7-methyl-2-oxo-N-(2,3,5,6-tetrafluoro-[1,1'-biphenyl]-4-yl)-1,2-

dihydropyrazolo[1,5-a]pyridine-3-carboxamide (22b). Obtained from **20b**, flash chromatography (eluent: *petroleum ether* / EtOAc 95:5 v/v). Pale yellow solid (m.p. 220.8 - 222.3 °C; from trituration with diisopropyl ether). Yield 41 %. ¹H NMR (600 MHz, CDCl₃): δ 2.67 (*s*, 3H, Ar-CH₃), 5.58 (*s*, 2H, -NCH₂Ph), 6.51 (*d*, 1H, *J* = 7.1 Hz, *H-b*), 6.94 (*d*, 2H, *J* = 6.7, *H-m*), 7.23 – 7.31 (*m*, 3H, *H-n*, *H-o*), 7.38 (*dd*, 1H, *J* = 8.8 Hz, 7.2 Hz, *H-c*), 7.43 – 7.53 (*m*, 5H, *aromatic protons*), 8.25 (*d*, 1H, *J* = 8.5 Hz, *H-d*), 10.07 (*s*, 1H, -NH); ¹³C NMR (151 MHz, CDCl₃): δ 20.7 (Ar-CH₃), 51.8 (-NCH₂Ph), 87.5 (*C-f*), 115.2 (*C-b*)*, 116.3 (*C-d*)*, 117.7, 126.1, 127.7, 128.5, 128.7, 129.1, 129.4, 130.4, 133.7 (*C-c*), 134.5 (*C-l*), 137.0, 138.9 (*C-a*), 143.3, 143.7, 148.2, 161.8 (*C-g*)*, 167.5 (*C-h*)*; MS (ESI) 506 (M+1). IR (KBr) ν (cm⁻¹): 3231, 3160, 3100, 3027, 2925, 1688, 1626, 1604, 1560, 1532, 1483, 1451, 1424, 1312, 1256, 1182, 1160, 1139, 1102, 1009, 982.

1-Benzyl-5-methyl-2-oxo-N-(2,3,5,6-tetrafluoro-[1,1'-biphenyl]-4-yl)-1,2-

dihydropyrazolo[1,5-a]pyridine-3-carboxamide (22c). Obtained from **20c**, flash chromatography (eluent: *petroleum ether* / EtOAc 90:10 v/v). Pale yellow solid (m.p. 200.7 - 202.7 °C; from trituration with diisopropyl ether). Yield 38 %. ¹H NMR (600 MHz, CDCl₃): δ 2.38 (*s*, 3H, Ar-CH₃), 5.44 (*s*, 2H, -NCH₂Ph), 6.57 (*dd*, 1H, *J* = 7.1 Hz, 1.7 Hz, *H-b*), 7.27 (*d*, 2H, *J* = 6.9, *H-m*), 7.34 (*t*, 1H, *J* = 7.3 Hz, *H-o*), 7.38 (*t*, 2H, *J* = 7.3 Hz, *H-n*), 7.43 – 7.53 (*m*, 5H, *aromatic protons*), 7.58 (*d*, 1H, *J* = 7.1 Hz, *H-a*), 8.11 (*s*, 1H, *H-d*), 10.07 (*s*, 1H, -NH); ¹³C NMR (151 MHz, CDCl₃): δ 21.6 (Ar-CH₃), 45.6 (-NCH₂Ph), 86.3 (*C-f*), 115.0 (*C-b*), 116.3, 117.3 (*C-d*), 117.5, 122.3 (*C-a*), 127.0, 127.7, 128.6, 128.8, 129.0, 129.6, 130.3, 132.8 (*C-l*), 142.5 (*C-c*), 143.4, 143.6, 144.0 (*C-e*), 161.8 (*C-g*)*, 162.6 (*C-h*)*; MS (ESI) 506

(M+1). IR (KBr) ν (cm⁻¹): 3233, 3101, 3066, 1672, 1653, 1631, 1528, 1487, 1438, 1311, 1242, 1176, 1126, 1076, 977.

General procedure for synthesis of pyrazolo[1,5-a]pyridine related amides 26 – 28. 2 M oxalyl chloride in dry dichloromethane (1.75 mL, 3.50 mmol) and dry DMF (1 drop) were added to a cooled (0° C) solution of **20a** (1.00 mmol) in dry THF (15 mL), under a nitrogen atmosphere. The reaction mixture was stirred for 2 hours at room temperature under a nitrogen atmosphere. The solution was concentrated under reduced pressure and the residue was dissolved in dry THF (10 mL, this step was repeated three times). The resulting acyl chloride was dissolved in dry toluene (15 mL). A solution of the appropriate aniline (1.00 mmol) and dry pyridine (3.00 mmol) in dry toluene (5 mL) was added dropwise to the solution of acyl chloride under nitrogen atmosphere. The resulting mixture was stirred at reflux overnight, then cooled to room temperature and quenched with 0.5 M HCl (25 mL). The layers were resolved, the aqueous phase was further extracted with EtOAc (3 x 50 mL), and the combined organic layer was washed with brine, dried and evaporated under reduced pressure. The crude material was purified using flash chromatography.

2-Benzyloxy-N-(4-phenoxyphenyl)pyrazolo[1,5-a]pyridine-3-carboxamide (26). Obtained from **20a**, using aniline **23**. Flash chromatography (eluent: dichloromethane / EtOAc 98:2 v/v). White solid (m.p. 170.6 - 171.3 °C; from trituration with diisopropyl ether). Yield 81 %. ¹H-NMR (300 MHz, CDCl₃): δ 5.52 (s, 2H, -OCH₂Ph), 6.80 (td, 1H, J = 6.9 Hz, 1.5 Hz, *H-b*), 6.90 (d, 4H, J = 8.8 Hz, *aromatic protons*), 6.99 (t, 1H, J = 7.4 Hz, *aromatic proton*), 7.16 - 7.53 (m, 11H, *aromatic protons*), 8.23 (d, 2H, J = 8.5 Hz, *aromatic protons*), 8.62 (s, 1H, -NH); ¹³C-NMR (151 MHz CDCl₃): δ 72.2 (-OCH₂Ph), 90.9 (*C-f*), 112.9 (*C-b*), 118.3, 118.9 (*C-d*), 120.0, 121.2, 122.9, 127.7 (*C-c*), 128.3, 128.7, 128.9 (*C-a*)*, 129.0, 129.8, 134.5, 135.8, 143.0, 152.7, 158.0, 161.2 (*C-h*)*, 162.2 (*C-g*)*; MS (ESI) 436 (M+1). IR (KBr) ν (cm⁻¹): 3379, 3059, 3039, 1661, 1636, 1545, 1532, 1487, 1464, 1364, 1307, 1223, 1150, 1127, 1103, 1010.

2-Benzyloxy-N-(2-methyl-4-phenoxy-phenyl)pyrazolo[1,5-a]pyridine-3-carboxamide

(27). Obtained from **20a**, using aniline **24**. Flash chromatography eluent: dichloromethane / EtOAc 98:2 v/v. Brown solid (m.p. 172.0 – 173.0 °C; from trituration with diisopropyl ether). Yield 97 %. ¹H-NMR (600 MHz, CDCl₃): δ 2.19 (s, 3H, Ar-CH₃), 5.57 (s, 2H, -OCH₂Ph), 6.85 - 6.89 (m, 4H, *aromatic protons*), 7.01 (t, 1H, J = 7.5 Hz, *aromatic protons*), 7.24 - 7.30 (m, 3H, *aromatic protons*), 7.35 - 7.49 (m, 5H, *aromatic protons*), 7.54 - 7.58 (m, 2H, *aromatic protons*), 8.29 - 8.33 (m, 2H, *aromatic protons*), 8.69 (s, 1H, -NH); ¹³C-NMR (151 MHz CDCl₃): δ 16.4 (Ar-CH₃), 72.2 (-OCH₂Ph), 90.9 (C-f), 112.8, 116.7, 118.4, 118.9, 120.9, 122.1, 122.6, 127.6, 128.2, 128.6, 128.9, 129.0, 129.7, 131.0, 135.0, 143.0 (C-e), 149.9, 158.5, 161.2 (C-h)*, 162.2 (C-g)*; MS (ESI) 450 (M+1). IR (KBr) ν (cm⁻¹): 3382, 3059, 3042, 1655, 1637, 1557, 1548, 1534, 1489, 1458, 1406, 1337, 1291, 1250, 1223, 1146, 1117, 997.

2-Benzyloxy-N-(2,5-dimethyl-4-phenoxy-phenyl)pyrazolo[1,5-a]pyridine-3-carboxamide

(28). Obtained from **20a**, using aniline **25**. Flash chromatography eluent: dichloromethane / EtOAc 98:2 v/v. Brown solid (m.p. 212.8 - 213.6 °C; from trituration with diisopropyl ether). Yield 98 %. ¹H-NMR (600 MHz, CDCl₃): δ 1.77 (s, 3H, Ar-CH₃), 2.18 (s, 3H, Ar-CH₃), 5.52 (s, 2H, -OCH₂Ph), 6.66 (s, 1H, *aromatic proton*), 6.82 - 6.90 (m, 3H, *aromatic protons*), 6.98 (t, 1H, J = 7.5 Hz, *aromatic proton*), 7.22 - 7.27 (m, 2H, *aromatic protons*), 7.34 - 7.43 (m, 4H, *aromatic protons*), 7.49 - 7.54 (m, 2H, *aromatic protons*), 8.17 (s, 1H, *aromatic proton*); 8.29 - 8.36 (m, 2H, *aromatic protons*), 8.42 (s, 1H, -NH); ¹³C-NMR (151 MHz CDCl₃): δ 16.2 (Ar-CH₃), 17.1 (Ar-CH₃), 72.6 (-OCH₂Ph), 91.1, 112.8, 116.8, 119.0, 122.0, 122.1, 124.4, 126.6, 127.6, 128.4, 128.7, 128.9, 129.2, 129.4, 129.7, 133.2, 135.4, 143.1 (C-e), 149.8, 158.6, 161.2 (C-h)*, 162.3 (C-g)*; MS (ESI) 464 (M+1). IR (KBr) ν (cm⁻¹): 3392, 3059, 3044, 2923, 2854, 1658, 1638, 1586, 1532, 1486, 1462, 1402, 1361, 1292, 1223, 1148, 1079, 1000.

General hydrogenation procedure for target compounds 4 - 6. Palladium on carbon (Pd/C, 6% w / w) was added to a solution of the appropriate amide (compounds **22a - c**, 1.0 mmol) in dry THF (15 mL) and 37 % HCl (1.0 mmol). The resulting mixture was vigorously stirred under a hydrogen atmosphere for 6 hours. The suspension was filtered through Celite and the cake was washed with methanol. The filtrate was concentrated under reduced pressure. When necessary, the obtained solid was further purified by flash chromatography.

2-Hydroxy-N-(2,3,5,6-tetrafluoro-[1,1'-biphenyl]-4-yl)pyrazolo[1,5-a]pyridine-3-carboxamide (4). Obtained from **22a**, flash chromatography (eluent: dichloromethane / EtOAc / HCOOH 80:20:1 v/v/v). Pale yellow solid (m.p. 260.9 - 262.0 °C dec.; from trituration with diisopropyl ether). Yield 87 %. ¹H NMR (600 MHz, DMSO): δ 6.93 (*t*, 1H, *J* = 6.7 Hz, *H-b*), 7.42 (*t*, 1H, *J* = 7.7 Hz, *H-c*), 7.48 – 7.63 (*m*, 5H, *aromatic protons*), 7.90 (*d*, 1H, *J* = 8.6 Hz, *H-d*), 8.51 (*d*, 1H, *J* = 6.6 Hz, *H-a*), 9.77 (*br s*, 1H, -NH). Exchangeable proton signals overlapped with the water signal. ¹³C NMR (151 MHz, DMSO): δ 88.9 (*C-f*), 112.9 (*C-b*), 116.6 (*C-d*), 117.1, 117.8, 127.3 (*C-c*), 127.9, 129.1 (*C-a*), 129.3, 129.8, 130.7, 142.1, 143.1, 143.8, 161.6 (*C-h*), 163.9 (*C-g*); MS (ESI) 402 (*M*+1). IR (KBr) ν (cm⁻¹): 3383, 3360, 2577, 1676, 1642, 1518, 1492, 1437, 1330, 1269, 1214, 1128, 994. ESI-HRMS (*m/z*) [*M* + *H*]⁺ calcd. for C₂₀H₁₂F₄N₃O₂ 402.0860, obsd. 402.0861.

2-Hydroxy-7-methyl-N-(2,3,5,6-tetrafluoro-[1,1'-biphenyl]-4-yl)pyrazolo[1,5-a]pyridine-3-carboxamide (5). Obtained from **22b**, flash chromatography (eluent: dichloromethane / EtOAc / HCOOH 80:20:1 v/v/v). White solid (m.p. 285.9 - 286.6 °C; from trituration with diisopropyl ether). Yield 86 %. ¹H NMR (600 MHz, DMSO): δ 2.65 (*s*, 3H, Ar-CH₃), 6.96 (*dd*, 1H, *J* = 6.9 Hz, 1.7 Hz, *H-b*), 7.46 (*t*, 1H *J* = 7.9 Hz, *H-c*), 7.53 – 7.66 (*m*, 5H, *aromatic protons*), 7.91 (*d*, 1H, *J* = 8.6 Hz, *H-d*), 8.94 (*s*, 1H, -NH); 12.95 (*br s*, 1H, -OH); ¹³C NMR (151 MHz, DMSO): δ 18.0 (Ar-CH₃), 88.8 (*C-f*), 113.3 (*C-b*), 115.0 (*C-d*), 117.6, 119.0, 127.2, 128.8 (*C-c*), 129.4, 129.9, 130.6, 138.8 (*C-a*), 142.6 (*C-e*), 143.5, 145.4, 161.1 (*C-h*), 163 (*C-g*); MS (ESI) 416 (*M*+1). IR (KBr) ν (cm⁻¹): 3379, 3012, 2600, 1697, 1644, 1574,

1548, 1526, 1493, 1439, 1311, 1245, 1167, 1131, 994. ESI-HRMS (m/z) [M + H]⁺ calcd. for C₂₁H₁₄F₄N₃O₂ 416.1017, obsd. 416.1018.

2-Hydroxy-5-methyl-N-(2,3,5,6-tetrafluoro-[1,1'-biphenyl]-4-yl)pyrazolo[1,5-a]pyridine-3-carboxamide (6). Obtained from **22c**, flash chromatography (eluent: dichloromethane / EtOAc / HCOOH 80:20:1 v/v/v). White solid (m.p. 287.1 – 287.5 °C dec.; from trituration with diisopropyl ether). Yield 83 %. ¹H NMR (600 MHz, DMSO): δ 2.39 (s, 3H, Ar-CH₃), 6.86 (dd, 1H, J = 6.9 Hz, 1.7 Hz, *H-b*), 7.49 – 7.60 (m, 5H, *aromatic protons*), 7.78 (s, 1H, *H-d*), 8.47 (d, 1H, J = 6.9 Hz, *H-a*), 8.95 (s, 1H, -NH). Exchangeable proton signals overlapped with the water signal. ¹³C NMR (151 MHz, DMSO): δ 21.0 (Ar-CH₃), 87.4 (*C-f*), 115.3 (*C-b*), 115.6 (*C-d*), 117.0, 126.7, 128.4, 128.8, 129.4 (*C-a*), 130.1, 139.3 (*C-c*), 141.7 (*C-e*), 144.2, 144.8, 160.4 (*C-h*), 163.0 (*C-g*); MS (ESI) 416 (M+1). IR (KBr) ν (cm⁻¹): 3381, 3362, 2992, 2590, 1677, 1648, 1517, 1491, 1437, 1334, 1275, 1224, 1123, 993. ESI-HRMS (m/z) [M + H]⁺ calcd. for C₂₁H₁₄F₄N₃O₂ 416.1017, obsd. 416.1019.

1-Methyl-2-oxo-N-(2,3,5,6-tetrafluoro-[1,1'-biphenyl]-4-yl)-1,2-dihydropyrazolo[1,5-a]pyridine-3-carboxamide (7). 5 M NaOH (1 eq.) was added to a solution of compound **17a** (600 mg, 2.73 mmol) in ethanol (20 mL). The solution was stirred for 3 hours at 70 °C, then concentrated under reduced pressure to get, in a quantitative yield, the corresponding acid sodium salt **17b**, which was dried and used in the next step without any further purification. 2 M Oxalyl chloride in dry DCM (2.45 mL, 4.90 mmol), and dry DMF (1 drop), were added to a cooled (0 °C), solution of **17b** (350 mg, 1.63 mmol), in dry THF (25 mL), under a nitrogen atmosphere and the resulting solution was stirred at room temperature for 2 hours. The solution was then concentrated under reduced pressure and the residue dissolved in dry THF (10 mL, this step was repeated three times), giving the corresponding acyl chloride, which was immediately used without any further purification. Trimethylaluminium (2.0 M in hexane, 1.86 mL, 3.72 mmol) was added to a solution of 2,3,5,6-tetrafluoro-4-phenylaniline **21** (394 mg, 1.96 mmol) in dry toluene (15 mL), under a nitrogen atmosphere. The resulting

mixture was stirred for 2 hours at room temperature resulting in a brown suspension, which was quantitatively transferred portionwise to a solution of acyl chloride, raised from the previous steps, in dry toluene (30 mL). The mixture was heated overnight at 90 °C, cooled to r.t. then quenched with 1 M HCl. The layers were resolved and the aqueous phase exhaustively extracted with ethyl acetate. The combined organic layer was washed with 1 M NaOH and brine, dried and the solvent was evaporated under reduced pressure. The crude product was purified by column chromatography (*petroleum ether* / EtOAc from 8:2 to 6:4 v/v) to afford the title compound as a pale yellow solid. Yield 27 %. ¹H NMR (300 MHz, DMSO): δ 3.70 (*s*, 3H, -NCH₃), 7.22 (*t*, 1H, *J* = 6.5, *H-b*), 7.46 - 7.63 (*m*, 5H, *aromatic protons*), 7.76 (*t*, 1H, *J* = 7.9, *H-c*), 8.06 (*d*, 1H, *J* = 8.7 Hz, *H-d*), 8.73 (*d*, 1H, *J* = 6.9 Hz, *H-a*), 10.10 (*s*, 1H, -NH); ¹³C NMR (75 MHz, DMSO): δ 28.5 (-NCH₃), 85.8 (*C-f*), 113.3 (*C-b*), 116.1 (*C-d*), 117.1, 125.2 (*C-a*), 127.1, 129.1, 129.6, 130.4, 132.5, 140.9, 141.1, 144.2, 144.4, 161.2 (*C-g*)*, 161.8 (*C-h*)*; MS (ESI) 416 (M+1).

General hydrogenation procedure for target compounds 8 – 10. Palladium on carbon (Pd/C, 45 mg) was added to a solution of the appropriate amide (compounds **26 - 28**, 0.300 mmol) in dry THF (15 mL). The resulting mixture was vigorously stirred under a hydrogen atmosphere for 3 hours. The suspension was filtered through Celite and the cake was washed with methanol. The filtrate was concentrated under reduced pressure. When necessary, the obtained solid was further purified by flash chromatography.

2-Hydroxy-N-(4-phenoxyphenyl)pyrazolo[1,5-a]pyridine-3-carboxamide (8). Obtained from **26**, flash chromatography (eluent: dichloromethane / EtOAc / HCOOH 85:15:1 v/v/v). Brown solid (m.p. 147.6 - 148.2°C; from trituration with diisopropyl ether). Yield 80 %. ¹H-NMR (600 MHz, DMSO): δ 6.91 – 7.05 (*m*, 5H, *aromatic protons*), 7.10 (*t*, 1H, *J* = 7.3 Hz, *H-b*), 7.37 (*t*, 2H, *J* = 7.9 Hz, *aromatic protons*), 7.46 (*t*, 1H, *J* = 7.9 Hz, *H-c*), 7.70 (*d*, 2H, *J* = 8.9 Hz, *aromatic protons*), 8.05 (*d*, 1H, *J* = 8.7 Hz, *H-d*), 8.56 (*d*, 1H, *J* = 6.8 Hz, *H-a*), 9.05 (*s*, 1H, -NH), 12.77 (*br s*, 1H, -OH); ¹³C-NMR (151 MHz DMSO): δ 89.3 (*C-f*), 112.7

(C-b), 117.0 (C-d), 117.9, 119.5, 121.0, 122.9, 127.6 (C-c), 128.9 (C-a), 129.9, 134.7, 141.5 (C-e), 151.6, 157.4, 160.8 (C-h)*, 161.9 (C-g)*; MS (ESI) 346 (M+1). IR (KBr) ν (cm⁻¹): 3370, 3036, 2571, 1661, 1602, 1544, 1505, 1490, 1449, 1335, 1260, 1231, 1124, 1103, 983. ESI-HRMS (m/z) [M + H]⁺ calcd. for C₂₀H₁₆N₃O₃ 346.1186, obsd. 346.1184.

2-Hydroxy-N-(3-methyl-4-phenoxyphenyl)pyrazolo[1,5-a]pyridine-3-carboxamide (9).

Obtained from **27**, flash chromatography (eluent: dichloromethane / EtOAc / HCOOH 80:20:1 v/v/v). Brown solid (m.p. 233.7 - 235.9 °C dec.; from trituration with diisopropyl ether). Yield 85 %. ¹H-NMR (600 MHz, DMSO): δ 2.14 (s, 3H, Ar-CH₃), 6.83 – 6.94 (m, 3H, aromatic protons), 6.98 (td, 1H, J = 7.0 Hz, 1.3 Hz, H-b), 7.04 (t, 1H, J = 7.4 Hz, aromatic proton), 7.33 (dd, 2H, J = 8.4 Hz, 7.6 Hz, aromatic protons), 7.47 (t, 1H, J = 7.9 Hz, H-c), 7.56 (dd, 1H, J = 8.7 Hz, 2.5 Hz, aromatic proton), 7.63 (d, 1H, J = 2.2 Hz, aromatic proton), 8.06 (d, 1H, J = 8.7 Hz, H-d), 8.57 (d, 1H, J = 6.8 Hz, H-a), 9.04 (s, 1H, -NH), 12.82 (br s, 1H, -OH); ¹³C-NMR (151 MHz DMSO): δ 16.8 (Ar-CH₃), 90.2 (C-f), 113.7 (C-b), 117.2, 117.9 (C-d), 119.3, 121.5, 123.0, 123.1, 128.6 (C-c), 129.8 (C-a), 130.7, 130.8, 136.2, 142.4 (C-e), 149.7, 158.8, 161.7 (C-h)*, 162.8 (C-g)*; MS (ESI) 360 (M+1). IR (KBr) ν (cm⁻¹): 3387, 3061, 2572, 1666, 1638, 1534, 1488, 1328, 1226, 1130, 1107, 932. ESI-HRMS (m/z) [M + H]⁺ calcd. for C₂₁H₁₈N₃O₃ 360.1343, obsd. 360.1337.

N-(2,5-Dimethyl-4-phenoxyphenyl)-2-hydroxypyrazolo[1,5-a]pyridine-3-carboxamide

(10). Obtained from **28**, flash chromatography (eluent: dichloromethane / EtOAc / HCOOH 80:20:1 v/v/v). Brown solid (m.p. 249.1 - 254.2 °C dec.; from trituration with diisopropyl ether). Yield 67 %. ¹H-NMR (600 MHz, DMSO): δ 2.12 (s, 3H, Ar-CH₃), 2.24 (s, 3H, Ar-CH₃), 6.73 - 7.10 (m, 5H, aromatic protons, H-b)), 7.33 (t, 2H, J = 7.7 Hz, aromatic protons), 7.48 (t, 1H, J = 7.4 Hz, aromatic proton), 7.33 (dd, 2H, J = 8.4 Hz, 7.6 Hz, aromatic protons), 7.48 (t, 1H, J = 7.8 Hz, H-c), 8.08 (d, 1H, J = 8.7 Hz, H-d), 8.19 (s, 1H, aromatic proton), 8.58 (d, 1H, J = 6.6 Hz, H-a), 9.04 (s, 1H, -NH), 13.00 (br s, 1H, -OH); ¹³C-NMR (151 MHz DMSO): δ 16.7 (Ar-CH₃), 17.9 (Ar-CH₃), 90.3 (C-f), 113.7 (C-b), 117.1, 117.9

(C-d), 122.9, 123.0, 124.2, 127.1(C-c), 127.9 (C-a), 128.6, 129.8, 130.7, 134.5, 142.3 (C-e), 149.4, 158.9, 161.5 (C-h)*, 162.9 (C-g)*; MS (ESI) 374 (M+1). IR (KBr) ν (cm⁻¹): 3395, 2926, 2582, 1670, 1640, 1550, 1487, 1440, 1402, 1331, 1193, 1078. ESI-HRMS (m/z) [M + H]⁺ calcd. for C₂₂H₂₀N₃O₃ 374.1499, obsd. 374.1501.

4.2. Molecular modeling

4.2.1. Protein preparation. All analyses were conducted on the *h*DHODH protein conformation that was extracted from the X-ray data using PDB ID: 5MUT. The missing protein loops were built and the crystal structure of the protein underwent an optimization process using the Protein Preparation Wizard tool, implemented in MaestroTM GUI.⁴¹ Missing hydrogen atoms were added and bond orders were assigned. The prediction of protonation states for the protein was accomplished using PROPKATM, with the pH set at 7.4.

4.2.2. Missing loops refinement. Missing loops (amino acids 69-72 and 212-226) in the *h*DHODH protein were filled in using the MODELLER 9.11 package in order to obtain a complete protein structure.⁴² Two other *h*DHODH proteins (PDB ID: 4IGH and 4OQV) were used as templates for the missing loops. The best model was selected according to DOPE score.

4.2.3. Docking. Docking studies on the compounds shown herein were performed using Glide/Inducet Fit Docking Protocol (IFD).⁴³ Docking was performed using the bound crystallographic ligand as the centroid of the box. The standard IFD protocol was used. Protein preparation constrained refinement and Glide XP redocking were set, while the other parameters were kept in their default states.

4.2.4. Molecular dynamics. Molecular dynamic simulations were performed using GROMACS (version 5.0.5).⁴⁴ The parameter files for the complexes were prepared using the tLeap module of Ambertools and the amber ff14SB force field.^{45, 46} Ligand and cofactor (Flavin mononucleotide and Orotate), parameters were obtained using the Antechamber

module⁴⁷ and AM1-BCC charge methods.⁴⁸ The starting structures were immersed in a pre-equilibrated cubic box of around 25000 TIP3P water molecules and chloride ions were added to maintain the electrical neutrality of the simulated systems. The systems were minimized over 6000 steps of the steepest descent algorithm before MD simulations were performed. The minimized structures were used as a starting point for the MD simulations. During the equilibration steps, the protein α carbons were kept fixed with a constraint of 1000 kcal/mol. In the first step, a constant volume simulation (NVT), was performed, during which the system was heated from 0 to 300 K over three 100-ps steps; 100, 200 and 300 K. The second, isothermal- and isobaric ensemble (NPT), was performed using the Parrinello-Rahman algorithm for 1 ns of dynamic simulation. Finally, 50 ns MD production trajectories were run without restraint, collecting frames at 100 ps intervals and using a 2 fs time step. Particle mesh Ewald (PME),⁴⁹ was used to treat the long-range electrostatic interactions in MM minimization and MD simulations. All bonds were constrained using the LINCS algorithm.⁵⁰

4.2.5. MD trajectory clustering. The MD trajectory of compounds **4**, **8**, **9** and **10**, in their complexes with *h*DHODH, were clustered using *CPPTRAJ* from Ambertools in order to retrieve the average structures.. Best-fit coordinate RMSDs were calculated using ligand heavy atoms as references and a distance cutoff of 1 Å for cluster forming.

4.2.6. Free binding energy calculations. Molecular mechanics/generalized born surface area (MM/GBSA) is a widely used technique to calculate the binding free energy between receptor and ligand.⁵¹⁻⁵³ Here, the MM/GBSA method was employed to compute the binding free energy of DHODH in complex with compounds **4**, **8**, **9**, **10**. The free energies were calculated on basis of the last 40 ns of MD trajectories. The ΔG_{bind} of protein-ligand complexes were computed with the following equation:

$$\Delta G_{\text{bind}} = \Delta H - T \Delta S \approx \Delta E_{\text{MM}} + \Delta G_{\text{sol}} - T \Delta S$$

$$\Delta E_{\text{MM}} = \Delta E_{\text{internal}} + \Delta E_{\text{ele}} + \Delta E_{\text{vdw}}$$

$$\Delta G_{so} = \Delta G_{GB} + \Delta G_{SA}$$

where ΔE_{MM} , T ΔS and ΔG_{sol} represent the gas phase MM energy, conformational entropy, and solvation free energy, respectively. ΔE_{MM} consists of van der Waals energy ΔE_{vdw} , electrostatic ΔE_{ele} and $\Delta E_{internal}$ of the bond, angle, and dihedral energies. The Generalized Born (GB) model was used to compute the polar solvation free energies ΔG_{GB} .⁵⁴ And, the LCPO method was employed to calculate the nonpolar solvation contribution energy ΔG_{SA} .⁵⁵ To compute the entropy calculation, 400 snapshots were extracted from the simulated trajectories every 100 ps. All binding free energy calculations were carried out by AmberTools14 and AMBER14.⁴⁶ MMPBSA.py program were used to decompose the contribution energies of individual residues.⁵⁶

4.2.7. FEP analysis. All simulations were performed in GROMACS (version 5.0.5), more details are provided in the supplementary material section. Two different sets of calculations were performed for each alchemical transformation; one on the ligand-protein solvated complex and the other on the ligand into the solvent. FESetup⁵⁷ was used to prepare the input. Free energies were obtained via the implementation of multiple Bennet acceptance ratios (MBAR), which were provided by python package pymbar (<https://github.com/choderalab/pymbar>),⁵⁸ using the Alchemical analysis tool (<https://github.com/MobleyLab/alchemical-analysis>).⁵⁹

4.3. Protein expression and purification. The cDNA of the N-truncated form of *h*DHODH (aa31 - 395), was amplified from a full length *h*DHODH I.M.A.G.E. clone (ID 6064723), and inserted into a pFN2A vector (Promega). The vector produces *h*DHODH as an N-terminal GST-fusion protein. The plasmid pFN2A-*h*DHODH was transformed into BL21 (DE3), *pyrD E. coli* cells for protein production. Cells were grown at 37 °C in LB medium supplemented with 0.1 mM flavin mononucleotide. After 20 h of growth, cells were induced with 0.4 mM isopropyl-D-thiogalactopyranoside at an OD₆₀₀ of 0.6 - 0.8 at 28 °C for an additional 3 h. A cell pellet from 300 mL of culture was lysed in 20 ml of PBS (50 mM

Na₂HPO₄, 50 mM NaH₂PO₄, 500 mM NaCl), which had been supplemented with 24 mg lysozyme and 0.2 % v/v protease inhibitor cocktail (Sigma-Aldrich), incubated for 30 min over ice and disrupted by sonication. Triton X-100 was added to the lysate, to a final concentration of 1 %, before centrifugation at 14000 × g for 40 min at 4 °C. The clarified supernatant was incubated with DNase I (Sigma Aldrich), for 30 min at room temperature, supplemented with 2 mM DTT and filtered through a 0.45 µm syringe filter. The GST-fused enzyme was purified from the bacterial lysate using affinity chromatography on immobilized glutathione-sepharose columns and fast protein liquid chromatography (FPLC). The GST tag was not removed for further studies.

4.4. *h*DHODH inhibition assay. Inhibitory activity was assessed by monitoring the reduction of 2,6-dichloroindophenol (DCIP), which is associated with the oxidation of dihydroorotate as catalyzed by the DHODH enzyme. The enzyme was preincubated for five minutes at 37 °C in Tris-buffer solution (pH 8.0), with coenzyme Q10 (100 µM), with the compounds to be tested used at different concentrations (final DMSO concentration 0.1 % v/v), with DCIP (50 µM). The reaction was initiated by the addition of DHO (500 µM), and the reduction was monitored at $\lambda = 650$ nm. The initial rate was measured in the first five minutes ($\epsilon = 10400 \text{ M}^{-1}\text{cm}^{-1}$), and an IC₅₀ value was calculated,⁶⁰ using GraphPad Prism 7 software. Values are means \pm SE of three independent experiments.

4.5. Cell culture and drug treatment. Jurkat cells were cultured in X-VIVO 15 (BE02-060F, Lonza), supplemented with 10 % (v/v), fetal bovine serum (F-7524, Sigma Aldrich), and 1 % (v/v), antibiotic-antimycotic solution (A-5955, Sigma Aldrich) (complete medium). Cells were maintained at 37 °C in a 5 % CO₂ humidified atmosphere. Cells were passaged every 2–3 days and discarded after 15 passages. Jurkat cells were routinely tested, to confirm the absence of *mycoplasma*, using the MycoAlert Plus detection kit (Lonza), and were used for all experiments when in passages 5 and 10. Each compound tested was solubilized in

DMSO (drug vehicle, 41639, Fluka), at a final concentration of 10 mM, which was used as the stock solution for all experiments. Final dilutions were made in culture medium.

4.6. Proliferation assay. The growth of Jurkat T-cells was evaluated, via the quantitation of DNA content, using the fluorescent dye Hoechst 33258.⁶¹ Cells (5×10^3 in 100 μ L medium), were seeded in a white 96-well plate and exposed to increasing concentrations (0.001–200 μ M), of each compound or vehicle (DMSO), for 72 h. At the end of incubation, the medium was aspirated and the wells washed twice with 100 μ L phosphate buffer saline (137 mM NaCl, 2.7 mM KCl, 8.1 mM Na_2HPO_4 , 1.76 mM KH_2PO_4 , PH 7.4). Cells were exposed to 100 μ L 0.02 % SDS solution in SSC buffer (154 mM NaCl, 15 mM sodium citrate, pH 7), for 1 h at 37 °C with occasional swirling. At the end of the process, an equal volume of 1 μ g/mL Hoechst 33258 solution in SSC buffer was added to each well and fluorescence measured at 355 nm (excitation), and 460 nm (emission), using a Fluoroskan Ascent-Thermo microplate fluorometer (Thermo Fisher Scientific, MA). IC₅₀ values were determined using nonlinear regression plots on GraphPad Prism6. Values are means \pm SE of three independent experiments. Where indicated, the antiproliferative effect was evaluated in the presence of 100 μ M uridine.³⁷

4.7 Cytotoxicity assay. The cytotoxic effects that the compounds had on Jurkat T cells were evaluated using the CellTox green assay (Promega). Cells (5×10^3 /well), were seeded in a white-opaque 96-well plate and exposed to increasing concentrations (0.001 - 100 μ M), of each compound or vehicle (DMSO), for 72 h. Values are means \pm SE of three independent experiments and represent the concentrations that cause significant (≥ 30 %), cytotoxic effects.

4.8. Immunosuppression assay. PBMCs were isolated via the Ficoll/Isopaque (Lymphoprep), density gradient centrifugation of buffy coat leukapheresis residues from the fresh blood samples of healthy donors. Purified cells were grown and maintained in culture medium at 37 °C in a 5 % CO₂ humidified atmosphere. Cells (5×10^3 /well), were seeded in a

white-opaque 96-well plate and exposed to increasing concentrations (0.001 - 100 μ M), of each compound or vehicle (DMSO), for 2 h and then stimulated with 1.25 mg/ml phytohemagglutinin (PHA) for 72 h. Cell proliferation was assessed via the quantitation of DNA content using the fluorescent dye Hoechst 33258, as described above. IC₅₀ values were determined using nonlinear regression plots on GraphPad Prism6. Values are means \pm SE of three independent experiments. Where indicated, the antiproliferative effect was evaluated in the presence of 100 μ M uridine.

4.9. Cell lines and drug treatment. Human cells THP1 (acute monocytic leukemia), and U937 (pro-monocytic myeloid leukemia), were cultured in complete RPMI 1640 (Invitrogen Life Technologies, Gaithersburg, MD), supplemented with 10 % heat-inactivated fetal bovine serum (FBS), and 1 % penicillin/streptomycin (GIBCO, Invitrogen, Milan, Italy).

4.10. Flow cytometric analysis. The expression of CD11b (PE-conjugated BD Bioscience San Jose, CA, USA), and CD14 (FITC-conjugated Beckam Coulter CA, USA), cell surface molecules was determined by flow cytometry analysis. Cells were washed and resuspended in staining buffer (phosphate-buffered saline, 2 % bovine serum albumin, 1mM EDTA), and incubated with antibodies at 4 °C for 45 min. Samples were acquired on a FACS Calibur and dead cells were excluded from the analyses, according to the use of propidium iodide (Sigma-Aldrich, Milan, Italy). Data were processed using Kaluza software version 1.2 (Beckman Coulter Fullerton, CA).

4.11. CFSE-based cytotoxic activity assay. Briefly, cell lines (THP1 and U937), were incubated with 2 mM carboxyfluorescein diacetate succinimidyl ester dye (CFSE, Vybrant CFDA SE cell tracer kit; Molecular Probes, Invitrogen Carlsbad, CA), at 107/ml for 20 min at 37 °C. At the end of the labeling process, cells were resuspended and washed in RPMI-1640 supplemented with 1 % fetal bovine serum. Then cells were resuspended in RPMI 1640 supplemented with 10 % FBS and incubated for 20 minutes at 37 °C. Cells were centrifuged and plated (1x10⁴ in 200 μ l of medium), with increasing concentrations of *h*DHODH

inhibitors (0.01 μ M to 10 μ M), for 3 days. The same experiments were repeated in the presence of uridine 100 μ M. Cells were harvested and 1 μ g/ml of propidium iodide was added to assign the ratio of cell death. The percentage of specific lysis was calculated as described and in accordance with the following equation: $[\text{dead targets in sample (\%)} - \text{spontaneously dead targets (\%)}] / (100 - \text{spontaneously dead targets (\%)}) \times 100$. Spontaneous release was obtained by incubating cell lines in medium supplemented with the corresponding percentage of DMSO used for the dilution of compounds, whereas maximal release was obtained after treatment with triton solution.

4.12. Proliferation assay. The proliferation of AML cell lines (THP1 and U937), was evaluated using a flow cytometer. Cell lines were labeled with CFSE dye according to the protocol described above. After labeling, cell lines were plated (1×10^4), and cultured with *h*DHODH inhibitor molecules (0.01 μ M to 10 μ M), for three days. At the end of the cultures, cells were harvested and 1 μ g/ml of propidium iodide was added to exclude dead cells before acquisition. The proliferation of cell lines was quantified on viable cells as % of PI-CSFE-cells.

4.13. Differentiation assay. 1×10^4 cells (THP1 and U937), were plated in 96 well round-bottom plates and *h*DHODH inhibitors were added, from 0.1 μ M to 10 μ M, to a volume of 200 μ l of medium. The differentiation kinetics was monitored from day 1 to day 4 for U937, and to day 5 for THP1. Cells were washed and either stained with CD11b (U937), or with CD11b and CD14 (THP1), as described above. The differentiation assay was also performed in the presence of uridine 100 μ M and analyzed on day 3

4.14. Statistical analysis. Statistical analyses were performed on Prism software, version 5.0 (GraphPad Software, San Diego, CA). Data are reported as means \pm SD. Two tail paired Student's t tests were calculated to assess the differences between mean values and $P < 0.05$ was considered significant.

4.15. Solubility assay at pH 7.4. Solubility was assayed both in Phosphate Buffered Saline (PBS: 12 mM with NaCl 137 mM and KCl 2.7 mM, pH 7.4), and in PBS with DMSO (2 % V/V). Each solid compound (1 mg), was added to 1 mL of PBS or PBS/DMSO. The samples were shaken in an orbital shaker at 25 °C for 24 h. These suspensions were filtered through a PTFE 0.45 µm filter (VWR), and the solutions were chromatographically analyzed. Quantitative analysis was performed on a HPLC-UV system (MERK -HITACHI), equipped with an auto sampler of 60 µL injection volume (MERK-HITACHI AS-2000A), a binary HPLC pump (MERK-HITACHI L-6200 IP), and a diode array detector (MERK-HITACHI L-4250). LC analysis was performed using an Agilent Zorbax SB-Phenyl *Column* (4.6 x 250, 5 µm). Analyses were carried out at a flow rate of 1 mL/min using gradient elution with eluent A being trifluoroacetic acid (TFA), 0.1 % in water and B TFA 0.1% in MeOH for brequinar and compounds **4** - **10**. The analyses started with 40 % of eluent B and the following gradient profile was used: (time min, % B) 18.0, 100 %; 26.0, 100 %; 28.0, 40 %. For compound **5**, eluent A was TFA 0.1 % in water and eluent B acetonitrile. The gradient profile was as follows: (time, % B): 0, 50 %; 7.5, 50 %; 22.4, 100 %; 32.4, 100 %. Single compound quantification was made using the relative calibration curve, which was obtained by analyzing standard solutions in MeOH. Solubility is expressed as µM concentration of the saturated solution.

4.16. Clog P and log D (pH 7.4). ClogP values were calculated using the Bio-Loom program for Windows, Version 1.5 (BioByte). The partition coefficients between *n*-octanol and PBS at pH 7.4 ($\log D^{7.4}$), were obtained using the shake-flask technique at room temperature. In the shake-flask experiments, 50 mM of phosphate buffered saline pH 7.4 was used as the aqueous phase. The organic (*n*-octanol), and aqueous phases were mutually saturated by shaking for 4 h. The compounds were solubilized in the buffered aqueous phase at the highest concentration compatible with solubility and appropriate amounts of *n*-octanol were added. The two phases were shaken for about 20 min, by which time the partitioning equilibrium of

solutes had been reached, and then centrifuged (10000 rpm, 10 min). The concentration of the solutes was measured in the aqueous phase by UV spectrophotometer (Varian Cary 50BIO); absorbance values (recorded for each compound at the wavelength of maximum absorption), were interpolated in calibration curves obtained using standard solutions of the compounds ($r^2 > 0.99$). Each log D value is an average of at least six measurements.

4.17. Serum stability. A solution of the selected compound in DMSO was added to human serum (sterile-filtered from human male AB plasma, Sigma-Aldrich), to obtain the desired final concentration with 2 % of co-solvent. The resulting solution was shaken in an orbital shaker at 37 °C for 24 h. At appropriate time intervals (0, 0.5, 1, 4 and 24 hours), 300 µL of the reaction mixture were withdrawn and added to 600 µL of trifluoroacetic acid (TFA), 0.1% in acetonitrile in order to deproteinize the serum. The samples were vortexed, sonicated for 3 min and then centrifuged for 5 min at 2500 x g. The clear supernatant was filtered and analyzed by RP-HPLC. HPLC analyses were performed on a HP 1100 chromatograph system (Agilent Technologies, Palo Alto, CA, USA), equipped with a quaternary pump (model G1311A), a membrane degasser (G1379A), and a diode-array detector (DAD) (model G1315B), integrated into the HP1100 system. Data analyses were processed using a HP ChemStation system (Agilent Technologies). The analytical column was a ZORBAX Eclipse XDB-C18 (4.6 × 150 mm, 5 µm, Agilent Technologies). The mobile phase consisted of acetonitrile 0.1 % TFA / water 0.1 % TFA 70/30 v/v at flow-rate = 1.0 mL/min. The injection volume was 20 µL (Rheodyne, Cotati, CA). The column effluent was monitored at 245 and 264 nm referenced against a 700 nm wavelength. Single compound quantification was achieved using calibration curves that were obtained by analyzing standard solutions. The results are expressed as % of unmodified parent compound at 24 h.

4.18. Protein binding *in vitro*. Free- and protein-bound drug separation was achieved by ultrafiltration using commercially available membrane systems (Centrifree ultrafiltration devices with ultracel YM-T membrane, Merck). A solution of selected compound in DMSO

was added to human serum (sterile-filtered from human male AB plasma, Sigma-Aldrich), to obtain the desired final concentration with 2 % of co-solvent. 1 mL of the solution obtained from the sample reservoir of the ultrafiltration device was gently shaken in an orbital shaker at 37 °C for 1 h. The tube was then centrifuged at 1000 x g for 25 min. The concentrations of the compounds in the ultrafiltrate and filtrate were determined using reverse-phase HPLC and the chromatographic conditions described above. The quantitation of the compounds in the filtrate was performed using the calibration curves of compound standard solutions (linearity determined in a concentration range of 1-100 µM; $r^2 > 0.99$). The quantitation of compounds in the ultrafiltrate was performed using calibration curves obtained from the method of standard addition (linearity determined in a concentration range of 0-2.5 µM; $r^2 > 0.99$). The recovery of the ultrafiltration process was calculated in order to discover whether any compound was lost during ultrafiltration, considering the limited solubility of tested compounds.

$$\text{Recovery} = 100 \times [(\text{vol.}_{\text{bound}} \times \text{conc}_{\text{bound}}) + (\text{vol.}_{\text{unbound}} \times \text{conc}_{\text{unbound}})] / \text{vol}_{\text{initial serum}} \times \text{conc}_{\text{initial}}$$

$\text{vol.}_{\text{bound}}$: calculated by dividing the weight of the bound fraction (difference between the weights of the sample reservoir after ultrafiltration and empty), by its density (0.991 g/mL assessed by weighing five replicates of a known volume of bound fraction).

$\text{vol.}_{\text{unbound}}$: calculated by dividing the weight of the unbound fraction (difference between the weights of the ultrafiltrate cup after and before ultrafiltration), by its density (0.999 g/mL assessed by weighing five replicates of a known volume of unbound fraction).

$\text{conc}_{\text{bound}}$: calculated using the RP-HPLC method.

$\text{conc}_{\text{unbound}}$: calculated using the RP-HPLC method (calibration with standard additions)

Medium recovery was 97 % for all tested compounds.

4.19. Protein expression, purification and crystallization. A N-terminally truncated *h*DHODH (Met30-Arg396) (N10XHis-*h*DHODH30-396) construct was expressed and purified as previously described.¹⁴ For crystallization, the purified protein was mixed with ORO (final concentration 2 mM) and compound **4** (final concentration 2 mM) from 50 mM stocks dissolved in DMSO and subsequently incubated at room temperature for one hour. The crystallization trials were performed using MRC 2 well sitting drop plates (Molecular Dimensions Limited) with a Mosquito robot (TTP Labtech). 300 nL protein pre-incubated with inhibitor and ORO was mixed 300 nL reservoir solution consisting of 0.2 M KBr, 0.2 M KSCN, 0.1M NaOAc pH 5.0, 25 - 35 % v/v PEG 400, 2 - 5% v/v PGA-LM (Molecular Dimension Limited). As the formation of the desired cubic crystal form varied from time to time with crowding agent concentrations, a grid with concentrations varying between 25 - 35 % v/v PEG 400 and 2 - 5 % (v/v) PGA-LM was set up during the crystallization. Trays were incubated at 20 °C for 7 days after which crystals were flash-cooled in liquid nitrogen.

4.20. X-ray data collection, structure determination and refinement. X-ray diffraction data were collected at 100 K on beamline ID23- 1 at European Synchrotron Radiation Facility (ESRF), France using a Pilatus detector. The data were indexed, integrated and scaled using the iMosflm and Scala utilities of the CCP4 program suit.⁶² The structure was determined by molecular replacement with PHASER⁶³ using the structure of DHODH¹⁴ as a search model. Multiple rounds of simulated annealing were performed to minimize model bias. The final model was built with Coot⁶⁴ and refined with Phenix⁶⁵ to a resolution of 1.58 Å with the final R_{work} and R_{free} values of 0.1368 and 0.1597, respectively. Data collection and refinement statistics are summarized in Table S1. The coordinates have been deposited in the Protein Data Bank (PDBID: 6FMD).

5. ACKNOWLEDGEMENTS

This research was supported by funds from the University of Turin, Ricerca Locale 2015 and 2016 (grant numbers LOLM_RILO_17_01, BOSD_RILO_17_01) and PRIN 2015

(LOLM_PRIN_2015_16_01). The authors wish to thank Dr. Livio Stevanato for performing all the NMR experiments and for instrument maintenance and Dr. Dale James Matthew Lawson for proofreading the final manuscript. In particular, the authors would like to thank prof Francesca Spyarakis (UniTO) for fruitful discussions on the modeling part of the study.

6. PDB CODES

The coordinates of compound **4** in complex with human DHODH have been deposited in the Protein Data Bank (PDBID: 6FMD) and the authors will release the atomic coordinates and experimental data upon article publication.

7. ASSOCIATED CONTENT

Supporting Information: a PDF file containing: MD/FEP analysis; X-ray data collection and refinement statistics; determination of the main physicochemical properties Clog P, log D (pH 7.4) and pKa for compounds **15a**, **16a**, **17a**, **18a** and **19a**; Jurkat T cell stability assay, 2D-NMR characterization compounds **16a**, **17a**, **18a** and **19a**; Synthesis of compounds **24** and **25** and characterization; ¹H-NMR and ¹³C-NMR spectra of representative compounds. (PDF). Molecular formula strings and biological data (CSV).

8. ABBREVIATIONS USED

*h*DHODH: *human* dihydroorotate dehydrogenase, DHO: dihydroorotate, ORO: orotate, AML: acute myelogenous leukemia, HOSA: hydroxylamine-O-sulfonic acid, RMSD: root mean square deviations, MD: Molecular dynamics, PHA: phytohaemagglutinin, PBMCs: peripheral blood mononuclear cells, CFSE: carboxyfluorescein diacetate succinimidyl ester, TFA: trifluoroacetic acid, FEP: free-energy perturbation. FEB: free energy of binding. PRED: pre-residue energy decomposition

9. AUTHOR INFORMATION

Corresponding Author

*Phone: +39 0116707180. Fax: +39 0116707162. E-mail: marco.lolli@unito.it

ORCID Marco Lucio Lolli: 0000-0002-3030-3163

Notes

The authors declare no competing financial interest

10. BIBLIOGRAPHY

1. Leban, J.; Vitt, D. Human Dihydroorotate Dehydrogenase Inhibitors, a Novel Approach for the Treatment of Autoimmune and Inflammatory Diseases. *Arzneimittelforschung* **2011**, 61, 66-72.
2. Vyas, V. K.; Variya, B.; Ghate, M. D. Design, Synthesis and Pharmacological Evaluation of Novel Substituted Quinoline-2-Carboxamide Derivatives as Human Dihydroorotate Dehydrogenase (hDHODH) Inhibitors and Anticancer Agents. *Eur J Med Chem* **2014**, 82, 385-393.
3. Lolli, M. L.; Sainas, S.; Pippione, A. C.; Giorgis, M.; Boschi, D.; Dosio, F. Use of Human Dihydroorotate Dehydrogenase (hDHODH) Inhibitors in Autoimmune Diseases and New Perspectives in Cancer Therapy. *Recent Pat Anticancer Drug Discov* **2018**, 13, 86-105.
4. Munier-Lehmann, H.; Vidalain, P. O.; Tangy, F.; Janin, Y. L. On Dihydroorotate Dehydrogenases and Their Inhibitors and Uses. *J Med Chem* **2013**, 56, 3148-3167.
5. Herrmann, M. L.; Schleyerbach, R.; Kirschbaum, B. J. Leflunomide: an Immunomodulatory Drug for the Treatment of Rheumatoid Arthritis and other Autoimmune Diseases. *Immunopharmacology* **2000**, 47, 273-289.
6. Singh, A.; Singh, P. Teriflunomide: a Novel Oral Disease-Modifying Agent Under Investigation for the Treatment of Multiple Sclerosis. *J. Drug Deliv. Ther.* **2016**, 6, 97-102.
7. Peters, G. J.; Sharma, S. L.; Laurensse, E.; Pinedo, H. M. Inhibition of Pyrimidine De Novo Synthesis by DUP-785 (NSC 368390). *Invest New Drugs* **1987**, 5, 235-244.
8. de Forni, M.; Chabot, G. G.; Armand, J. P.; Fontana, X.; Recondo, G.; Domenge, C.; Carde, P.; Barbu, M.; Gouyette, A. Phase I and Pharmacokinetic Study of Brequinar (DUP 785; NSC 368390) in Cancer Patients. *Eur J Cancer* **1993**, 29A, 983-988.
9. Joshi, A. S.; King, S. Y.; Zajac, B. A.; Makowka, L.; Sher, L. S.; Kahan, B. D.; Menkis, A. H.; Stiller, C. R.; Schaeffle, B.; Kornhauser, D. M. Phase I Safety and Pharmacokinetic Studies of Brequinar Sodium after Single Ascending Oral Doses in Stable Renal, Hepatic, and Cardiac Allograft Recipients. *J Clin Pharmacol* **1997**, 37, 1121-1128.
10. Schwartzmann, G.; Dodion, P.; Vermorken, J. B.; ten Bokkel Huinink, W. W.; Joggi, J.; Winograd, B.; Gall, H.; Simonetti, G.; van der Vijgh, W. J.; van Hennik, M. B.; et al. Phase I Study of Brequinar Sodium (NSC 368390) in Patients with Solid Malignancies. *Cancer Chemother Pharmacol* **1990**, 25, 345-351.
11. Sykes, D. B.; Kfoury, Y. S.; Mercier, F. E.; Wawer, M. J.; Law, J. M.; Haynes, M. K.; Lewis, T. A.; Schajnovitz, A.; Jain, E.; Lee, D.; Meyer, H.; Pierce, K. A.; Tolliday, N. J.; Waller, A.; Ferrara, S. J.; Eheim, A. L.; Stoeckigt, D.; Maxcy, K. L.; Cobert, J. M.; Bachand, J.; Szekely, B. A.; Mukherjee, S.; Sklar, L. A.; Kotz, J. D.; Clish, C. B.; Sadreyev, R. I.; Clemons, P. A.; Janzer, A.; Schreiber, S. L.; Scadden, D. T. Inhibition of Dihydroorotate Dehydrogenase Overcomes Differentiation Blockade in Acute Myeloid Leukemia. *Cell* **2016**, 167, 171-186.
12. Lewis, T. A.; Sykes, D. B.; Law, J. M.; Munoz, B.; Rustiguel, J. K.; Nonato, M. C.; Scadden, D. T.; Schreiber, S. L. Development of ML390: A Human DHODH Inhibitor that Induces Differentiation in Acute Myeloid Leukemia. *ACS Med Chem Lett* **2016**, 7, 1112-1117.
13. Tzelepis, K.; Koike-Yusa, H.; De Braekeleer, E.; Li, Y.; Metzakopian, E.; Dovey, O. M.; Mupo, A.; Grinkevich, V.; Li, M.; Mazan, M.; Gozdecka, M.; Ohnishi, S.; Cooper, J.; Patel, M.; McKerrell, T.; Chen, B.; Domingues, A. F.; Gallipoli, P.; Teichmann, S.

- Ponstingl, H.; McDermott, U.; Saez-Rodriguez, J.; Huntly, B. J. P.; Iorio, F.; Pina, C.; Vassiliou, G. S.; Yusa, K. A CRISPR Dropout Screen Identifies Genetic Vulnerabilities and Therapeutic Targets in Acute Myeloid Leukemia. *Cell Rep* **2016**, 17, 1193-1205.
14. Sainas, S.; Pippione, A. C.; Giorgis, M.; Lupino, E.; Goyal, P.; Ramondetti, C.; Buccinna, B.; Piccinini, M.; Braga, R. C.; Andrade, C. H.; Andersson, M.; Moritzer, A. C.; Friemann, R.; Mensa, S.; Al-Kadaraghi, S.; Boschi, D.; Lolli, M. L. Design, Synthesis, Biological Evaluation and X-Ray Structural Studies of Potent Human Dihydroorotate Dehydrogenase Inhibitors Based on Hydroxylated Azole Scaffolds. *Eur J Med Chem* **2017**, 129, 287-302.
 15. Gradl, S. N.; Nguyen, D.; Eis, K.; Gunther, J.; Stellfeld, T.; Janzer, A.; Sven, C.; Mueller, T.; El Sheikh, S.; Zhou, H. J.; Zhao, C.; Sykes, D. B.; Ferrara, S. J.; Liu, K.; Kröber, M.; Merz, C.; Niehues, M.; Schäfer, M.; Zimmermann, K.; Nising, C. F. 2,4,5-Trisubstituted 1,2,4-Triazolones Useful as Inhibitors of DHODH. May 03, 2018, WO 2018/077923 A1
 16. Li, S.; Luan, G.; Ren, X.; Song, W.; Xu, L.; Xu, M.; Zhu, J.; Dong, D.; Diao, Y.; Liu, X.; Zhu, L.; Wang, R.; Zhao, Z.; Xu, Y.; Li, H. Rational Design of Benzyldenehydrazinyl-Substituted Thiazole Derivatives as Potent Inhibitors of Human Dihydroorotate Dehydrogenase with in Vivo Anti-arthritic Activity. *Sci Rep* **2015**, 5, 14836 - 14855.
 17. Munier-Lehmann, H.; Lucas-Hourani, M.; Guillou, S.; Helynck, O.; Zanghi, G.; Noel, A.; Tangy, F.; Vidalain, P. O.; Janin, Y. L. Original 2-(3-Alkoxy-1H-pyrazol-1-yl)pyrimidine Derivatives as Inhibitors of Human Dihydroorotate Dehydrogenase (DHODH). *J Med Chem* **2015**, 58, 860-877.
 18. Zhu, J.; Han, L.; Diao, Y.; Ren, X.; Xu, M.; Xu, L.; Li, S.; Li, Q.; Dong, D.; Huang, J.; Liu, X.; Zhao, Z.; Wang, R.; Zhu, L.; Xu, Y.; Qian, X.; Li, H. Design, Synthesis, X-Ray Crystallographic Analysis, and Biological Evaluation of Thiazole Derivatives as Potent and Selective Inhibitors of Human Dihydroorotate Dehydrogenase. *J Med Chem* **2015**, 58, 1123-1139.
 19. Lucas-Hourani, M.; Munier-Lehmann, H.; El Mazouni, F.; Malmquist, N. A.; Harpon, J.; Coutant, E. P.; Guillou, S.; Helynck, O.; Noel, A.; Scherf, A.; Phillips, M. A.; Tangy, F.; Vidalain, P. O.; Janin, Y. L. Original 2-(3-Alkoxy-1H-pyrazol-1-yl)azines Inhibitors of Human Dihydroorotate Dehydrogenase (DHODH). *J Med Chem* **2015**, 58, 5579-5598.
 20. Lolli, M. L.; Giorgis, M.; Tosco, P.; Foti, A.; Fruttero, R.; Gasco, A. New Inhibitors of Dihydroorotate Dehydrogenase (DHODH) Based on the 4-Hydroxy-1,2,5-oxadiazol-3-yl (Hydroxyfurazanyl) Scaffold. *Eur J Med Chem* **2012**, 49, 102-109.
 21. Pippione, A. C.; Giraudo, A.; Bonanni, D.; Carnovale, I. M.; Marini, E.; Cena, C.; Costale, A.; Zonari, D.; Pors, K.; Sadiq, M.; Boschi, D.; Oliaro-Bosso, S.; Lolli, M. L. Hydroxytriazole Derivatives as Potent and Selective Aldo-keto Reductase 1C3 (AKR1C3) Inhibitors Discovered by Bioisosteric Scaffold Hopping Approach. *European Journal of Medicinal Chemistry* **2017**, 139, 936-946.
 22. Lolli, M. L.; Giordano, C.; Pickering, D. S.; Rolando, B.; Hansen, K. B.; Foti, A.; Contreras-Sanz, A.; Amir, A.; Fruttero, R.; Gasco, A.; Nielsen, B.; Johansen, T. N. 4-Hydroxy-1,2,5-oxadiazol-3-yl Moiety as Bioisoster of the Carboxy Function. Synthesis, Ionization Constants, and Molecular Pharmacological Characterization at Ionotropic Glutamate Receptors of Compounds Related to Glutamate and its Homologues. *J Med Chem* **2010**, 53, 4110-4118.
 23. Pippione, A. C.; Dosio, F.; Ducime, A.; Federico, A.; Martina, K.; Sainas, S.; Frolund, B.; Gooyit, M.; Janda, K. D.; Boschi, D.; Lolli, M. L. Substituted 4-Hydroxy-1,2,3-Triazoles: Synthesis, Characterization and First Drug Design Applications Through Bioisosteric Modulation and Scaffold Hopping Approaches. *MedChemComm* **2015**, 6, 1285-1292.
 24. Pippione, A. C.; Carnovale, I. M.; Bonanni, D.; Sini, M.; Goyal, P.; Marini, E.; Pors, K.; Adinolfi, S.; Zonari, D.; Festuccia, C.; Wahlgren, W. Y.; Friemann, R.; Bagnati, R.; Boschi, D.; Oliaro-Bosso, S.; Lolli, M. L. Potent and Selective Aldo-Keto Reductase 1C3

- (AKR1C3) Inhibitors Based on the Benzoisoxazole Moiety: Application of a Bioisosteric Scaffold Hopping Approach to Flufenamic Acid. *Eur J Med Chem* **2018**, 150, 930-945.
25. Baumgartner, R.; Walloschek, M.; Kralik, M.; Gotschlich, A.; Tasler, S.; Mies, J.; Leban, J. Dual Binding Mode of a Novel Series of DHODH Inhibitors. *J Med Chem* **2006**, 49, 1239-1247.
 26. Johnson, T. W.; Gallego, R. A.; Edwards, M. P. Lipophilic Efficiency as an Important Metric in Drug Design. *J Med Chem* **2018**, in press.
 27. Kakehi, A.; Ito, S.; Konno, Y.; Maeda, T. Synthesis Using PyridiniumN-Ylides. I. Synthesis and Some Reactions of Substituted 1-(Acetylimino)pyridinium Ylides. *B Chem Soc JPN* **1978**, 51, 251-256.
 28. Ochi, H.; Miyasaka, T.; Kanada, K.; Arakawa, K. Studies of Heterocyclic Compounds. VIII. Synthesis and Tautomerism of 2-Hydroxypyrazolo[1,5-a]pyridine. *B Chem Soc JPN* **1976**, 49, 1980-1984.
 29. Minkin, V. I.; Garnovskii, A. D.; Elguero, J.; Katritzky, A. R.; Denisko, O. V. The Tautomerism of Heterocycles: Five-membered Rings with Two or More Heteroatoms. In *Advances in Heterocyclic Chemistry*, Katritzky, A. R., Ed. Academic Press: 2000; Vol. 76, pp 157-323.
 30. Pippione, A. C.; Federico, A.; Ducime, A.; Sainas, S.; Boschi, D.; Barge, A.; Lupino, E.; Piccinini, M.; Kubbutat, M.; Contreras, J.-M.; Morice, C.; Al-Karadaghi, S.; Lolli, M. L. 4-Hydroxy-N-[3,5-bis(trifluoromethyl)phenyl]-1,2,5-thiadiazole-3-carboxamide: a Novel Inhibitor of the Canonical NF- κ B Cascade. *MedChemComm* **2017**, 8, 1850-1855.
 31. Williams-Noonan, B. J.; Yuriev, E.; Chalmers, D. K. Free Energy Methods in Drug Design: Prospects of "Alchemical Perturbation" in Medicinal Chemistry. *J Med Chem* **2018**, 61, 638-649.
 32. Jorgensen, W. L. Efficient Drug Lead Discovery and Optimization. *Acc Chem Res* **2009**, 42, 724-733.
 33. Zeevaart, J. G.; Wang, L.; Thakur, V. V.; Leung, C. S.; Tirado-Rives, J.; Bailey, C. M.; Domaoal, R. A.; Anderson, K. S.; Jorgensen, W. L. Optimization of Azoles as Anti-Human Immunodeficiency Virus Agents Guided by Free-Energy Calculations. *J Am Chem Soc* **2008**, 130, 9492-9499.
 34. Cockroft, S. L.; Perkins, J.; Zonta, C.; Adams, H.; Spey, S. E.; Low, C. M.; Vinter, J. G.; Lawson, K. R.; Urch, C. J.; Hunter, C. A. Substituent Effects on Aromatic Stacking Interactions. *Org Biomol Chem* **2007**, 5, 1062-1080.
 35. Bonomo, S.; Tosco, P.; Giorgis, M.; Lolli, M.; Fruttero, R. The Role of Fluorine in Stabilizing the Bioactive Conformation of Dihydroorotate Dehydrogenase Inhibitors. *J Mol Model* **2013**, 19, 1099-1107.
 36. Das, P.; Deng, X.; Zhang, L.; Roth, M. G.; Fontoura, B. M.; Phillips, M. A.; De Brabander, J. K. SAR Based Optimization of a 4-Quinoline Carboxylic Acid Analog with Potent Anti-Viral Activity. *ACS Med Chem Lett* **2013**, 4, 517-521.
 37. Cherwinski, H. M.; Cohn, R. G.; Cheung, P.; Webster, D. J.; Xu, Y. Z.; Caulfield, J. P.; Young, J. M.; Nakano, G.; Ransom, J. T. The Immunosuppressant Leflunomide Inhibits Lymphocyte Proliferation by Inhibiting Pyrimidine Biosynthesis. *Journal of Pharmacology and Experimental Therapeutics* **1995**, 275, 1043-1049.
 38. Aungst, B. J.; Blake, J. A.; Rogers, N. J.; Dusak, B. A. Effects of Plasma Protein Binding Displacement on the Pharmacokinetics, Tissue and Tumor Concentrations and Efficacy of Brequinar, a Highly Protein-Bound Antitumor Agent. *J Pharmacol Exp Ther* **1990**, 253, 230-236.
 39. King, S. Y.; Agra, A. M.; Shen, H. S.; Chi, C. L.; Adams, D. B.; Currie, V. E.; Bertino, J. R.; Pieniaszek, H. J., Jr.; Quon, C. Y. Protein Binding of Brequinar in the Plasma of Healthy Donors and Cancer Patients and Analysis of the Relationship Between Protein Binding and Pharmacokinetics in Cancer Patients. *Cancer Chemother Pharmacol* **1994**, 35, 101-108.

40. Kunz, K.; Dunkel, R.; Greul, J. N.; Ilg, K.; Mansfield, D. J.; Moradi, W. A.; Seitz, T.; Dahmen, P.; Wachendorff-Neumann, U.; Voerste, A. Preparation of Phenoxyphenylamidine Derivatives as Fungicides. WO 2008/110313 A1, Sept 18, 2008.
41. **Schrödinger Release 2017-3:** Maestro, Schrödinger, LLC, New York, NY, 2017.
42. Sali, A.; Blundell, T. L. Comparative Protein Modelling by Satisfaction of Spatial Restraints. *J Mol Biol* **1993**, 234, 779-815.
43. Kujawski, J.; Bernard, M. K.; Jodlowska, E.; Czaja, K.; Drabinska, B. On the Interactions of Leflunomide and Teriflunomide Within Receptor Cavity-Nmr Studies and Energy Calculations. *J Mol Model* **2015**, 21, 105 - 117.
44. Abraham, M. J.; Murtola, T.; Schulz, R.; Páll, S.; Smith, J. C.; Hess, B.; Lindahl, E. Gromacs: High Performance Molecular Simulations Through Multi-Level Parallelism from Laptops to Supercomputers. *SoftwareX* **2015**, 1-2, 19-25.
45. Maier, J. A.; Martinez, C.; Kasavajhala, K.; Wickstrom, L.; Hauser, K. E.; Simmerling, C. ff14SB: Improving the Accuracy of Protein Side Chain and Backbone Parameters from ff99SB. *J Chem Theory Comput* **2015**, 11, 3696-3713.
46. D.A. Case; D.S. Cerutti; T.E. Cheatham, I.; T.A. Darden; R.E. Duke; T.J. Giese; H. Gohlke; A.W. Goetz; D. Greene; N. Homeyer; S. Izadi; A. Kovalenko; T.S. Lee; S. LeGrand; P. Li, C. L.; J. Liu, T. L.; R. Luo; D. Mermelstein; K.M. Merz; G. Monard; H. Nguyen; I. Omelyan; A. Onufriev; F. Pan; R. Qi; D.R. Roe; A. Roitberg; C. Sagui; C.L. Simmerling; W.M. Botello-Smith; J. Swails; R.C. Walker; J. Wang; R.M. Wolf; X. Wu; L. Xiao; York, D. M.; and P.A. Kollman. AMBER 2017. *University of California, San Francisco* (2017).
47. Wang, J.; Wang, W.; Kollman, P. A.; Case, D. A. Automatic Atom Type and Bond Type Perception in Molecular Mechanical Calculations. *J Mol Graph Model* **2006**, 25, 247-260.
48. Jakalian, A.; Jack, D. B.; Bayly, C. I. Fast, Efficient Generation of High-Quality Atomic Charges. AM1-BCC Model: II. Parameterization and Validation. *J Comput Chem* **2002**, 23, 1623-1641.
49. Essmann, U.; Perera, L.; Berkowitz, M. L.; Darden, T.; Lee, H.; Pedersen, L. G. A Smooth Particle Mesh Ewald Method. *J Chem Phys* **1995**, 103, 8577-8593.
50. Hess, B.; Bekker, H.; Berendsen, H. J. C.; Fraaije, J. G. E. M. LINCS: A Linear Constraint Solver for Molecular Simulations. *J Comput Chem* **1997**, 18, 1463-1472.
51. Hou, T.; Wang, J.; Li, Y.; Wang, W. Assessing the Performance of the MM/PBSA and MM/GBSA Methods. 1. The Accuracy of Binding Free Energy Calculations Based on Molecular Dynamics Simulations. *J Chem Inf Model* **2011**, 51, 69-82.
52. Xu, L.; Sun, H.; Li, Y.; Wang, J.; Hou, T. Assessing the Performance of MM/PBSA and MM/GBSA Methods. 3. The Impact of Force Fields and Ligand Charge Models. *J Phys Chem B* **2013**, 117, 8408-8421.
53. Genheden, S.; Ryde, U. The MM/PBSA and MM/GBSA Methods to Estimate Ligand-Binding Affinities. *Expert Opin Drug Discov* **2015**, 10, 449-461.
54. Bashford, D.; Case, D. A. Generalized Born Models of Macromolecular Solvation Effects. *Annu Rev Phys Chem* **2000**, 51, 129-152.
55. Weiser, J.; Shenkin, P. S.; Still, W. C. Approximate Atomic Surfaces from Linear Combinations of Pairwise Overlaps (LCPO). *J Comput Chem* **1999**, 20, 217-230.
56. Miller, B. R., 3rd; McGee, T. D., Jr.; Swails, J. M.; Homeyer, N.; Gohlke, H.; Roitberg, A. E. MMPBSA.py: An Efficient Program for End-State Free Energy Calculations. *J Chem Theory Comput* **2012**, 8, 3314-3321.
57. Loeffler, H. H.; Michel, J.; Woods, C. FESetup: Automating Setup for Alchemical Free Energy Simulations. *J Chem Inf Model* **2015**, 55, 2485-2490.
58. Shirts, M. R.; Chodera, J. D. Statistically Optimal Analysis of Samples from Multiple Equilibrium States. *J Chem Phys* **2008**, 129, 124105-124110.
59. Klimovich, P. V.; Shirts, M. R.; Mobley, D. L. Guidelines for the Analysis of Free Energy Calculations. *J Comput Aided Mol Des* **2015**, 29, 397-411.

60. Giorgis, M.; Lolli, M. L.; Rolando, B.; Rao, A.; Tosco, P.; Chaurasia, S.; Marabello, D.; Fruttero, R.; Gasco, A. 1,2,5-Oxadiazole Analogues of Leflunomide and Related Compounds. *Eur J Med Chem* **2011**, 46, 383-392.
61. Rao, J.; Otto, W. R. Fluorimetric DNA Assay for Cell Growth Estimation. *Anal Biochem* **1992**, 207, 186-192.
62. Collaborative Computational Project, N. The CCP4 Suite: Programs for Protein Crystallography. *Acta Crystallogr D Biol Crystallogr* **1994**, 50, 760-763.
63. Storoni, L. C.; McCoy, A. J.; Read, R. J. Likelihood-Enhanced Fast Rotation Functions. *Acta Crystallogr D Biol Crystallogr* **2004**, 60, 432-438.
64. Emsley, P.; Cowtan, K. Coot: Model-Building Tools for Molecular Graphics. *Acta Crystallogr D Biol Crystallogr* **2004**, 60, 2126-2132.
65. Adams, P. D.; Afonine, P. V.; Bunkoczi, G.; Chen, V. B.; Davis, I. W.; Echols, N.; Headd, J. J.; Hung, L. W.; Kapral, G. J.; Grosse-Kunstleve, R. W.; McCoy, A. J.; Moriarty, N. W.; Oeffner, R.; Read, R. J.; Richardson, D. C.; Richardson, J. S.; Terwilliger, T. C.; Zwart, P. H. PHENIX: a Comprehensive Python-Based System for Macromolecular Structure Solution. *Acta Crystallogr D Biol Crystallogr* **2010**, 66, 213-221.

Table of Contents Graphic

